FAA-RD-76-52, II

**Project Report**
**ATC-67**

# Radar Detection of Thunderstorm Hazards for Air Traffic Control: Volume II, Radar Systems

S.M. Sussman

7 October 1976

**Lincoln Laboratory**
MASSACHUSETTS INSTITUTE OF TECHNOLOGY
*LEXINGTON, MASSACHUSETTS*

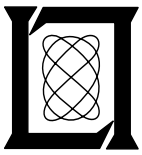

Prepared for the Federal Aviation Administration,
Washington, D.C. 20591

This document is available to the public through
the National Technical Information Service,
Springfield, VA 22161

Technical Report Documentation Page

| 1. Report No. | 2. Government Accession No. | 3. Recipient's Catalog No. |
|---|---|---|
| FAA-RD-76-52, II | | |

| 4. Title and Subtitle | 5. Report Date |
|---|---|
| Radar Detection of Thunderstorm Hazards for Air Traffic Control<br>Vol. II Radar Systems | 7 October 1976 |
| | 6. Performing Organization Code |
| 7. Author(s) | 8. Performing Organization Report No. |
| S. M. Sussman | ATC-67 |
| 9. Performing Organization Name and Address | 10. Work Unit No. (TRAIS) |
| Massachusetts Institute of Technology<br>Lincoln Laboratory<br>P. O. Box 73<br>Lexington, MA 02173 | 11. Contract or Grant No.<br>DOT-FA74WAI-485 |
| | 13. Type of Report and Period Covered |
| 12. Sponsoring Agency Name and Address | Project Report |
| Department of Transportation<br>Federal Aviation Administration<br>Systems Research and Development Service<br>Washington, DC 20591 | 14. Sponsoring Agency Code |

15. Supplementary Notes

The work reported in this document was performed at Lincoln Laboratory, a center for research operated by Massachusetts Institute of Technology under Air Force Contract F19628-76-C-0002.

16. Abstract


Radar systems are investigated for the acquisition of weather data to support detection and forecasting of hazardous turbulence associated with individual storm cells.

Utilization of the FAA Airport Surveillance Radar (ASR) is explored. The issues of antenna polarization and Sensitivity Time Control (STC) that impact on shared operation for aircraft and weather detection are addressed. Candidate system configurations employing a common RF channel and dual orthogonal polarization channels are discussed.

Ground clutter discrimination by coherent Doppler and noncoherent (Doppler spread) processing methods is described.

An interim procedure is suggested for obtaining fixed reflectivity contour data from a Moving Target Detector for use in the all-digital ARTS.

A preliminary design is presented for a new joint-use, long-range weather radar to support enroute air traffic controllers and to meet the data requirements of the National Weather Service and the Air Weather Service.


| 17. Key Words | | 18. Distribution Statement |
|---|---|---|
| Radar detection<br>weather radar<br>precipitative reflectivity | ground clutter<br>Doppler processing | Document is available to the public through the National Technical Information Service, Springfield, Virginia 22151 |

| 19. Security Classif. (of this report) | 20. Security Classif. (of this page) | 21. No. of Pages | |
|---|---|---|---|
| Unclassified | Unclassified | 72 | |

Form DOT F 1700.7 (8-72) Reproduction of completed page authorized

TABLE OF CONTENTS

TABLE OF CONTENTS (continued)

TABLE OF CONTENTS (continued)

LIST OF ILLUSTRATIONS

# 1.0 INTRODUCTION

## 1.1 The Need for Improved Radar Weather Data for Air Traffic Controllers

Severe weather, particularly that due to convective turbulence, can cause significant disruption to the safe, orderly flow of aircraft and correspondingly increases the work load for air traffic controllers. The impact of severe weather would be substantially reduced if controllers were presented a weather situation display showing the location of potentially hazardous regions associated with individual storm cells and a very short term forecast of the hazardous weather movement for 10 to 20 minutes into the future. This capability would allow controllers to preplan for pilot-requested course deviations and to issue weather advisories where necessary and would thereby enhance safety, reduce delays and decrease controller work load. The need for improved weather data for air traffic controllers is motivated in greater detail in Ref. 5 wherein the impact of weather on aircraft delays and accidents is addressed.

The radar weather images presently available to controllers fall far short of meeting the needs outlined above. The weather data are derived as a by-product of surveillance radars intended for aircraft target detection. The various techniques employed to enhance targets relative to ground and rain clutter, such as the use of circular polarization, Sensitivity-Time-Control (STC) and Moving Target Indication (MTI), all act to degrade the weather information presented to controllers. The display is in the form of wide areas of generally inaccurate weather reflectivity within which the smaller hazardous regions are not identifiable. Hence, controllers are often unaware of weather details visible to radar-equipped aircraft. The depiction of potentially hazardous turbulence provided on the ground should be at least as good as in the aircraft and should, in addition, include a very short term forecast presently unavailable in either location.

The wide disparity between air traffic controllers' radar weather needs and current capability led to the investigations on radar systems reported

## 1.2 Summary of Approach and Supporting Background

Recent studies reported in a companion volume [2]* have produced encouraging evidence that regions hazardous to aviation due to convective turbulence can be identified by precision measurement and processing of radar reflectivity maps. The rationale for this approach is the association of localized areas of vertical velocity fluctuations with the up drafts that produce rain showers and the subsequent down drafts that are produced as the storm cell matures. The up drafts provide the moisture to generate local regions of increased precipitation intensity which lead to relative maxima in reflectivity. The local reflectivity peaks can be detected as storm cells. Analysis of recorded data from the NASA SPANDAR radar at Wallops Island indicates that 1) storm cells are detectable with a reasonable probability of success, 2) they can be tracked over the cell lifetime of 10 to 40 minutes, and 3) their motion can be predicted from the track histories.

Evidence on the correlation between turbulence and reflectivity peaks is found in the literature on penetration flights through storms under observation by weather radar. In general there is a high correlation between the vertical velocity flucturations hazardous to aircraft and liquid water content, and, for lack of more detailed knowledge, pilots are advised to avoid regions of high radar reflectivity ( 40 dBZ)†. The regions with strong gusts are in general considerably smaller than the area within the fixed level contour, and some gusts are not associated with the main peak of reflectivity within the large echo area. Moreover, one finds gusts outside the regions of high reflectivity but within regions of detectable radar echo. Thus, the strategy of avoiding areas of high reflectivity reduces the potentially usable airspace and also occasionally fails to detect hazardous turbulence. Although the reported reflectivity measurements are not as precise as desired for cell determination, the location of at least some of the secondary reflectivity peaks can be estimated from the published contour data. The regions of reported turbulence along the flight paths predominantly fall in the vicinity of the primary and secondary peak locations.

---

*Number in brackets indicate references on p. 65.

†Z is a radar-independent measure of precipitation reflectivity [1].

Analyses reported in [2] also reveal that Doppler radar data, as could be acquired in a practical radar network, is not a direct measure for identifying aircraft hazards due to convective turbulence. As a supplement to, or in combination with, cell detection by reflectivity measurements, Doppler data may provide additional information for assessing aircraft hazards. The derivation of specific algorithms for accomplishing this and an evaluation of their effectiveness and practicality are unresolved issues. Radial Doppler signatures are known to be useful in identifying tornadoes and squalls that may cause surface wind damage, but these severe weather phenomena will also be associated with rain or hail cells detectable by reflectivity measurements. Doppler data, particularly from multiple radars with overlapping coverage, facilitates the study of large scale wind fields that carry precipitation. However, the processing of precision reflectivity maps as described here and in Reference 2 has the potential for detection of thunderstorm hazards of particular concern to air traffic controllers.

## 1.3 Summary of Report

This report documents the investigations on radar systems to meet the needs of air traffic controllers for radar weather data. The requirements imposed on the radar and associated processors to support individual storm cell detection and forecasting are reviewed. In the two environments, terminal and en route, two different sets of radar characteristics are appropriate.

In the terminal area where the desired coverage range is limited and where storm height information is not essential, the Airport Surveillance Radar (ASR) is a useful source of weather data. Several candidate methods are described to extract weather data from the ASR for storm cell detection and forecasting. These functions would be performed by a digital processor and in a mini-computer interfaced to the ARTS III display system.

The preferred ASR approach, excluding implementation cost factors, is a dual RF channel system employing two orthogonal polarization outputs from the antenna. The primary polarization signal that drives the aircraft channel may be switched from linear to circular to optimize target visibility in weather clutter. The weather channel accepts primary linear or opposite

sense circular to avoid the rain suppression and reflectivity uncertainty of same sense circular polarization. The dual channel configuration also permits separate optimization of Sensitivity Time Control (STC) thereby eliminating the necessity for compromising conflicting STC requirements. The ASR(8) has been specified with provision for an orthogonal polarization output through the rotary joint making the dual channel configuration directly applicable. Older radars would require retrofit of the feed system and rotary joint.

The anticipated implementation of advanced Moving Target Detectors (MTD) [3] for existing ASR's which do not have dual orthogonal polarization outputs and the reduced cost of a single processor, motivate consideration of a single RF channel configuration. Section 3.2 describes a method for expanding the processing functions of the MTD to produce weather data for cell detection and forecasting. Here linear antenna polarization is required for satisfactory weather data and circular polarization should be employed only when absolutely necessary. Although in tests at NAFEC the MTD has shown excellent target detectability in heavy rain using linear polarization, additional experimental evidence is necessary to claim that circular polarization can be eliminated. In the single channel system a compromise on STC must be reached to prevent excessive attenuation of weather echoes at close range while avoiding saturation of the A/D converters by strong ground clutter. Both polarization and STC choices are site dependent and no general conclusions can be drawn based on the evidence at hand. Additional effort is recommended to establish the suitability of the single channel configuration in meeting both aircraft and weather detection requirements.

In a dual channel configuration the weather processor could be of coherent or incoherent type. Since the cell detection mechanism does not utilize Doppler information, the main advantage of coherence is potential separability of weather and ground clutter due to radial storm velocity. The processing for coherent ground clutter suppression is similar to the operations of the MTD for which the potential separability of overlapping weather and ground clutter is realizable with around 50% probability for typical storms. When

relative radial motion is insufficient for distinguishability, the Doppler spectral spread can serve to discriminate between non-overlapping weather and ground clutter and hence to eliminate the latter from further processing. When an MTD is employed in the aircraft channel, parallel computations can be performed in the weather channel using a shared control structure. An integrated dual channel MTD processor of this form is described in Section 3.3.

A conventional ASR(8) in dual channel mode without MTD does not have the advantage of shared computation control for a coherent weather processor and is somewhat less effective in separating overlapping weather and ground clutter. These factors prompted consideration of a noncoherent weather processor using a logarithmic detector and relying only on Doppler spectral spread as a discriminant to eliminate ground clutter. A weather processor of this type is described in Section 3.2; it is suitable as an add-on to a standard ASR(8).

The achievement of a capability to display the present and future position of hazardous weather regions to controllers requires further effort on algorithm development, concept validation and implementation methods. Since these activities may lag the deployment of MTD and the all digital ARTS, an interim radar weather display should be available to replace the current analog video presentation. To accomplish this a procedure is described in Section 4.0 to extract weather data from the MTD for input to a contour generator, but it must be emphasized that this type of presentation does not satisfy the true needs of ATC controllers for identification and forecasts of small hazardous regions and also suffers from the above-cited conflicts between aircraft target and weather detection.

The storm height information required by en route controllers dictate the use of pencil beam radars. With their capability to detect weather at long range these radars can also serve the needs of the National Weather Service and Air Weather Service. Preliminary design parameters and issues of compatible shared operation for a joint use weather radar are discussed in Section 5.0. It is recommended that the radar operate at C-band with a 1°

beamwidth antenna to achieve adequate spatial resolution. In addition to the acquisition of reflectivity data to support ATC needs, coherent pulse-pair processing on a staggered pulse train is included to attain accurate unambiguous measurements of mean Doppler freqeuncy for analysis of radial wind fields by the other users. A sequence of nonuniformly spaced elevation tilt scans is suggested to acquire data automatically in the vertical dimension within the time limits imposed by the update rate required for cell tracking.

The report concludes with the following recommendations for future work to provide air traffic controllers with a display of the severe weather situation. The suggested steps are:

1. Develop a real-time demonstration system using an ASR to evaluate storm cell detection and forecasting for terminal controllers. To demonstrate weather processing only, the system need not be dual channel. A coherent processing capability with MTD-like filtering is desirable to minimize ground clutter effects.

2. Conduct weather radar and flight test experiments to confirm the turbulence/cell association, to refine forecast algorithms, and to explore the utility of Doppler information to improve hazard detection.(See Reference 2.)

3. Continue the investigation of single vs dual channel operation by determining the appropriateness of linear polarization for the MTD under extreme precipitation and by establishing compromise STC characteristics.

4. Estimate implementation costs of single vs dual channel configuration and coherent vs noncoherent processing. These comparisons will aid in the selection of the most cost effective approach.

5. Conduct a cost/benefit study to determine the expected cost and benefits that may accrue from implementation of the design alternatives.

6. Implement an interim capability to extract weather data from the MTD for the all-digital ARTS.

7. Coordinate with NWS and AWS on specifications for a new weather radar leading to a field demonstration test system that serves en route controllers and also provides the necessary data inputs for the other agencies.

## 2.0 RADAR REQUIREMENTS TO SUPPORT STORM CELL DETECTION AND FORECASTING

### 2.1 System Configuration

The basic configuration under consideration is shown in Fig. 2.1. The output from a more or less conventional radar is digitized and pre-processed to produce an estimate of reflectivity in suitably defined spatial resolution bins. A mini-computer accepts the data, performs storm cell detection and forecasts, and formats the resulting cell locations and other attributes for presentation on the controllers' graphic display. Depending on the geographical relationship of radar and ATC facilities, the computer functions may be divided between a radar on-site processor and a computer system at the controllers' location.

The following paragraphs state the requirements on the radar and associated processing system for potentially providing the controllers with the desired severe weather situation display. The requirements were derived from studies reported in the companion volume [2].

### 2.2 Precision and Accuracy

The successful detection of individual storm cells based on reflectivity peaks is dependent on clean data without significant distortion or extraneous maxima due to the fluctuations of the underlying random scattering phenomenon. Computer studies of cell detection algorithms indicate that 0.5 dB (rms) precision is satisfactory.

The precision is determined by the residual fluctuation in the estimate of reflectivity after a number of samples from the random (Rayleigh) process have been averaged. The mean and standard deviation of the sampled process is found in the literature for three types of video detectors: linear, square law and log magnitude. When N independent samples are averaged the standard deviation decreases inversely as $\sqrt{N}$. Table 2.1 gives the mean, standard deviation, and corresponding error expressed in terms of dB relative to mean reflectivity [7].

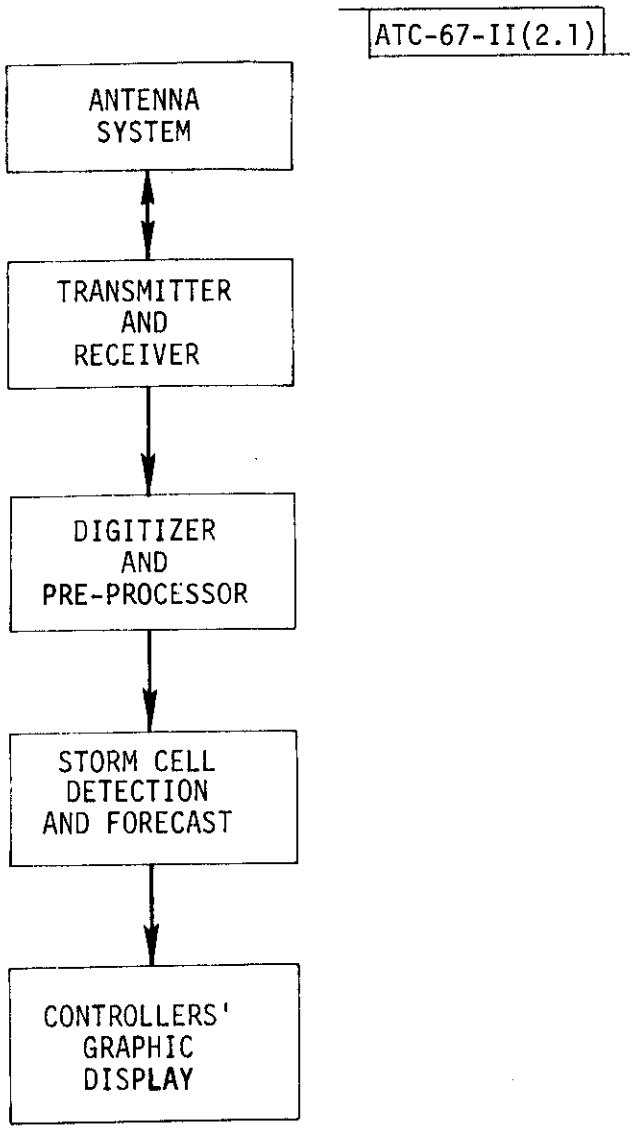


Fig. 2.1 Major elements of radar system to provide weather data for ATC.

TABLE 2.1

RAYLEIGH PROCESS STATISTICS

| Detector | Mean | Standard Deviation | dB Error |
|---|---|---|---|
| Square law | $\overline{A^2}$ | $\overline{A^2}/\sqrt{N}$ | $10 \log(1 \pm 1/\sqrt{N}) \approx \pm \frac{4.34}{\sqrt{N}}$ |
| Linear | $0.886 \sqrt{\overline{A^2}}$ | $0.463 \sqrt{\overline{A^2}}/\sqrt{N}$ | $20 \log(1 \pm 0.525/\sqrt{N}) \approx \pm \frac{4.54}{\sqrt{N}}$ |
| Logarithmic | $\log(0.561\ \overline{A^2})$ | $0.557/\sqrt{N}$ | $\pm \frac{5.57}{\sqrt{N}}$ |

With the square law detector for finite SNR in the samples, the result in the last column is modified to $4.34\ (1 + SNR^{-1})/\sqrt{N}$ (See App. B).

The desired 0.5 dB is attained with about 83 samples for linear or square law averaging at high SNR. The log magnitude averaging demands 50% more samples for the same precision. At 10 dB SNR the precision is degraded by 10% or the number of samples must be increased by 20% to keep it constant.

The absolute accuracy requirements are governed primarily by the necessity to assess cell severity from the echo intensity. A reasonable goal for accuracy is 5 dB combining radar calibration and beam filling errors.

## 2.3 Dynamic Range of Radar Reflectivity

Excluding the dependence of signal strength on range, the reflectivity of interest varies between 25 and 65 dBZ. These numbers correspond to mean values after averaging, hence another 5 dB should be added at both ends to allow for statistical fluctuations in the samples being averaged. The receiver dynamic range should therefore be 50 dB plus 30 to 40 dB for $(\text{range})^2$ dependence. If STC compensates for range dependence, then 50 to 55 dB dynamic range from noise floor to saturation is sufficient.

## 2.4 Update Interval and Processing Delay

The update interval is defined as the time between successive acquisitions of reflectivity data from any spatial resolution bin. The update rate must be fast enough to provide sample sequences of individual storm cells useful for tracking and forecast generation. The observed cell half-life is on the order of 10 to 15 minutes [2], hence the update interval should be no greater than 3 minutes, and preferably smaller.

Another factor related to the update interval is the delay from the time the data is first acquired to the time it appears on a controller display. This delay encompasses processing as well as transmission functions. Because of these delays what is presented to the controller as "current conditions" is actually a forecast from acquisition time to display time.

Let $T_u$ be the update interval and $T_p$ the processing delay. A new image is available for display $T_p$ after acquisition. The image about to be replaced is based on data acquired $T_p + T_u$ earlier. Therefore, the maximum forecast time for "current conditions" is $T_p + T_u$. It is important that this forecast be accurate since it will be compared to aircraft real-time observations during pilot-controller interactions. An upper limit of 6 minutes for the forecast range is reasonable.

The selection of $T_u$ and $T_p$, within the constraints $T_u < 3$ min. and $T_u + T_p < 6$ min., depends on the system design trade-offs between speed of acquisition and processing. The best choice may be different for terminal and en route implementations.

## 2.5 Spatial Resolution

Examination of storm cells in the available data base indicates that the most probable cell size is 3 km in horizontal diagonal dimension and that over 80% of severe cells are larger than 2 km [2].

A range resolution of 1 km is satisfactory to locate a cell and establish its radial extent. In the cross-range (azimuth) dimension the resolution is limited by practical considerations of beamwidth as discussed in the next subsection.

As for the vertical dimension, storm cell height information is required by en route controllers since aircraft under their jurisdiction may overfly convective turbulence retions. In the terminal control areas storm cells may only be avoided by horizontal course deviations, and consequently storm top data is not essential [5]. For a radar with an elevation scan capability, the storm height resolution depends on the range, the beamwidth and the elevation angle. A reasonable objective for height resolution is 2 km with maximum tops at 8 km.

## 2.6 Ground Clutter Suppression

To avoid confusion of ground clutter and anomalous propagation echoes with storm cells, mechanisms should be provided for rejecting the unwanted signals. Several levels of processing are possible toward attaining this objective. 1) Stationary ground clutter echoes can be eliminated on the basis of cell track histories; 2) the difference in Doppler spread between ground and weather echoes can serve as a criterion for distinguishing between the two when the echoes are spatially separated; 3) the radial velocity of weather echoes permits weather extraction by Doppler filtering for a fraction of overlapping situations (see Appendix A). The first two and possibly all three techniques are necessary for satisfactory storm cell detection and tracking in a ground clutter environment.

The use of a clutter map to remove ground clutter from the weather processing has also been suggested but is not favored for the following reasons. In the absence of precipitation, this technique would be equivalent to elimination of stationary cells as in mechanism (1) above. When ground clutter and weather echoes overlap, the two signals combine additively in power, so that power subtraction is called for. Subtracting the clutter map power from the combined echo power leads to weather reflectivity estimates which are subject to large errors resulting from the subtraction of two potentially large numbers, each with its own statistical inaccuracy. Furthermore, the ground clutter map should not be corrupted by weather echoes. Hence the map must be updated only in the absence of precipitation. This implies a decision mechanism to determine whether a change in echo power in a particular resolution bin is due to weather or a variation in ground clutter. Neither the subtraction accuracy nor the clutter update problem is amenable to simple solution.

## 2.7 Beamwidth and Range Considerations

Reflectivity accuracy and spatial resolution requirements determine the effective operating range for a radar with a given beamwidth. Two cases are considered: the existing surveillance radars and a new long range weather radar.

As stated above, the en route controllers require storm height data, hence the long range radars (LRR) with elevation fan beam antennas are not a suitable source of weather data. Even if this requirement were lifted, the LRR operating range would be limited by the loss in accuracy incurred through partial beam filling.

This error comes about when a cell of low height only partially fills the elevation beam. The reflected energy is interpreted as though the beam were completely filled and consequently the reflectivity is underestimated. A 3 dB contribution to the accuracy budget has been allocated to beam filling error.

Assuming an elevation beam cut-off at 4.8°, corresponding to an ASR(8) antenna tilted up by half a beamwidth, the range at which a cell of nominal 3.5 km height half fills the beam is 75 km. This range is comparable to the coverage of the Airport Surveillance Radar (ASR); it falls far short of the required coverage for en route radars.

At 75 km the 1.35° azimuth beamwidth of the ASR provides a cross-range resolution of 1.8 km a value consistent with the storm cell dimensions. Thus the ASR is a viable source of radar weather data for terminal controllers.

The en route requirements for weather data can be met with a pencil beam weather radar. A beamwidth of 1° allows an operating range of 180 km with a beam filling error of 3 dB on a 3.5 km high storm cell. The cross-range error at 180 km is 3.1 km, slightly larger than the most likely cell size but still acceptable. A radar with these characteristics could also serve the needs of the National Weather Service (NWS) and the Air Weather Service (AWS).

Preliminary designs for the ASR modification and a new joint use weather radar are addressed in the following chapters.

## 3.0 ASR MODIFICATION FOR STORM CELL DETECTION

### 3.1 Single vs. Dual RF Channel

One of the first issues that must be faced in designing a weather data extractor for the ASR is how much of the aircraft target receiver system can be shared for weather detection. The major conflicts discussed in detail below arise in the requirements on antenna polarization and STC characteristics.

#### 3.1.1 Linear vs. Circular Polarization

For aircraft targets the choice of polarization revolves around the enhancement in target signal relative to weather clutter necessary to achieve satisfactory target detectability. Although the aircraft cross-section with linear polarization is often larger by more than 3 dB compared to circular [13], it is common practice to employ circular polarization during periods of rain so as to gain an improvement of 10 to 15 dB due to reduced precipitation reflectivity [12].

The weather clutter suppression capability of the MTD is considerably better than conventional MTI radars as has been demonstrated during tests at NAFEC on a highly modified FPS-18.[10]. The FPS-18, which is very similar to an ASR-8, was run with linear polarization rather than circular polarization. The heaviest rain encountered at NAFEC during these tests was about 1/2" per hour. At that rate, linear polarization used in conjunction with the MTD was adequate to suppress the rain and still have excellent detectability on all aircraft in the coverage. In some areas of the country the rainfall rate is at times significantly greater than 1/2" (12.5 mm) per hour. It remains to be measured experimentally whether or not the MTD will work adequately in a linear polarization mode in such high rainfall rates.

On the other hand, the measurement of precipitation reflectivity imposes specific constraints on the choice of polarization. If linear polarization is employed on transmit, the same linear polarization is required on receive. If circular polarization is transmitted, the opposite sense circular is needed on receive. The circular polarization sense that suppresses rain not only reduces

the weather-to-noise ratio but also introduces large errors in reflectivity estimates because the rain cross section is strongly dependent on drop shape.

The requirements for both aircraft and weather detection can be met by a dual RF channel system in which the two opposite sense circular polarizations are brought out from the antenna. A switching arrangement can then apply the appropriate signal to the weather channel in accordance with the selected polarization.

### 3.1.2 Sensitivity Time Control

STC gain control is an essential feature of a linear digital radar processor to achieve the necessary overall dynamic range. Linear processing stages and A/D converters have a dynamic range less than the overall requirement and must be preceded by STC to avoid saturation. The form of STC characteristic depends on the distance dependence of both the desired target signal strength and the interfering echoes such as clutter and birds.

A point target with $R^{-4}$ echo power dependence on range R leads to $R^4$ gain characteristic. Except for gain variation due to the elevation pattern, this will maintain a constant SNR* for constant cross-section over the active STC range. Clutter, whose distance dependence is slower than $R^{-4}$, is then subject to greater attenuation at short ranges thereby minimizing A/D saturation by strong clutter. An important benefit of $R^4$ STC is that the MTD operating with a noise dependent threshold can discriminate against birds since weak targets, even at close range, rarely rise above the detection level.

For weather detection the desired signal power varies as $R^{-2}$ assuming complete beam filling. When this signal is amplified by $R^4$ gain, the net result is an $R^2$ signal variation. Consequently the weather SNR decreases with decreasing range in the active STC region.

A compatible STC for both weather and aircraft demands a limit on how far out in range the $R^4$ STC applies to assure that the weather SNR is adequate for reliable processing. To establish the STC range limit denoted by $R_c$, we consider the weather power budget for an ASR(8) shown in Table 3.1.

*SNR refers to receiver noise if STC is the first active receiver stage. If STC follows RF amplification, SNR refers to A/D quantization noise.

TABLE 3.1

S-BAND REFLECTIVITY POWER BUDGET

$$P_r = \frac{\pi^3 P_t G^2 \theta\phi\, h}{1024\, \lambda^2 \ln 2} \frac{|K|^2}{r^2} Z \quad \text{(Battan [1] p. 42)}$$

| | | | |
|---|---|---|---|
| $\pi^3/(1024 \ln 2)$ | = | 0.0437 | -13.6 dB |
| Transmitter Power, $P_t$ | = | 1 Mw | +90.0 dB mW |
| Gain, $G^2$ | | | 67.0 dB |
| Az beam. $\theta$ = 1.35° | = | 0.0236 rad | -16.3 dB rad |
| El beam, $\phi$ = 4.8° | = | 0.0838 rad | -10.8 dB rad |
| Pulse Length, h(0.6 μs) | = | 180 m | 22.6 dB m |
| Wavelength, $\lambda^{-2}$ | = | $(0.1\ m)^{-2}$ | 20.0 dB $m^{-2}$ |
| Maximum Range, $r^{-2}$ | = | $(75{,}000\ m)^{-2}$ | -97.5 dB $m^{-2}$ |
| Constant*, $\|K\|^2$ | = | $(0.935)^2$ | -1.2 dB |
| Reflectivity, Z(27 dBz $mm^6/m^3$) | | | -153 dB $m^3$ |
| Rotary Joint and Waveguide Losses | | | -0.7 dB |
| Atmospheric Loss | | | -1.0 dB |
| Receiver Power, $\overline{P_r}$ | | | -94.5 dB mW |
| Ref Noise Density, $kT_o$ | | | -114 dB mW $(MHz)^{-1}$ |
| Bandwidth, B = 2 MHz | | | 3 dB MHz |
| Noise Figure | | | 4 dB |
| | | | -107 dB mW |
| SNR per pulse at maximum range | | | 12.5 dB |

*Related to the index of refraction. See Reference 1.

The formula for received power taken from the referenced text assumes guassian-shaped beam patterns and complete beam filling.

Significant storm cells may have reflectivity as low as 30 dBZ. To permit measurements 3 dB down from peaks of this intensity a value of 27 dBZ has been selected as the minimum reflectivity of interest. This yields an SNR per pulse of 12.5 dB at the maximum range. Assuming the ASR incorporates Doppler filtering to improve ground clutter elimination, coherent averaging over a sequence of pulses (8 in the MTD) enhances the SNR by an amount dependent on the degree of signal correlation between successive pulses. Or stated differently, the SNR enhancement is determined by the spectral spread in relation to the frequency resolution achievable in one coherent processing interval. For constant signal the full coherent gain of 8 pulses is obtained. If the spectral spread covers, say, 3 frequency resolution cells, proper design will yield an SNR improvement of about 8/3 or 4.3 dB. Adding the last quantity to the per-pulse SNR gives an effective SNR per reflectivity sample of 16.8 dB at 75 km under the stated conditions.

The minimum acceptable SNR per sample is 10 dB. This is based in part on the considerations of the number of independent samples that must be averaged to achieve the desired estimate variance. The number of samples is proportional to $[1 + (SNR)^{-1}]^{-2}$, hence 10 dB SNR requires 20% more samples than the noiseless case. Also this SNR allows a small margin for unaccounted losses, e.g., less coherent averaging improvement due to larger Doppler spread. (Under the assumption in the preceding paragraph the SNR per pulse before Doppler filtering is only 5.7 dB.)

The point where 10 dB SNR is reached can be derived as a function of the range $R_c$ (km) where the $R^4$ STC terminates, i.e., where the receiver reaches full gain. The SNR for minimum reflectivity precipitation located at $R_c$ may be expressed relative to the 16.8 dB SNR found above at the 75 km maximum range by

$$(SNR)_c = 16.8 + 20 \log (75/R_c)$$

At closer ranges under $R^4$ STC the SNR is

$$SNR = 16.8 + 20 \log(75/R_c) - 20 \log(R_c/R)$$

$$= 54.3 + 20 \log R - 40 \log R_c$$

A minimum operating range of 4 km should be maintained to permit accurate observation in the vicinity of an airport of storm cells typically 2-4 km in diameter. Setting SNR = 10 and R = 4 results in $R_c$ = 25.7. Therefore the maximum extent of $R^4$ STC action is 25.7 km or 13.9 nmi. Site adaption of STC should remain within this limit under single RF channel operation of aircraft and weather detection.

NAFEC, where the MTD was tested, has very light ground clutter and moderate bird (angel) activity. With this mild environment a 48 dB $R^4$ STC was used which dropped off to zero attenuation at 9.5 miles. In more normal and in extreme clutter environments an $R^4$ STC which terminates at 25 to 30 nautical miles may be necessary to maintain the good aircraft detection and false alarm performance of the MTD [10]. This represents a weather SNR degradation of 10.2 to 13.4 dB at the minimum range or an increase in the latter to 13.0 and 18.7 km respectively.

Unless a compromise can be found where both aircraft and weather detection incur some loss in performance, STC considerations also point toward dual RF channel operation with separate optimization in each channel.

## 3.2 Single Channel Configuration

### 3.2.1 Overall System Structure

A block diagram of a possible future ASR system when weather and aircraft detection share the same RF channel is given in Fig. 3.1. After Doppler filtering in accordance with an MTD algorithm, a branch to a reflectivity preprocessor for weather is indicated. Although shown as functionally separate, the operations may actually be performed by the same processing elements that also do aircraft detection.

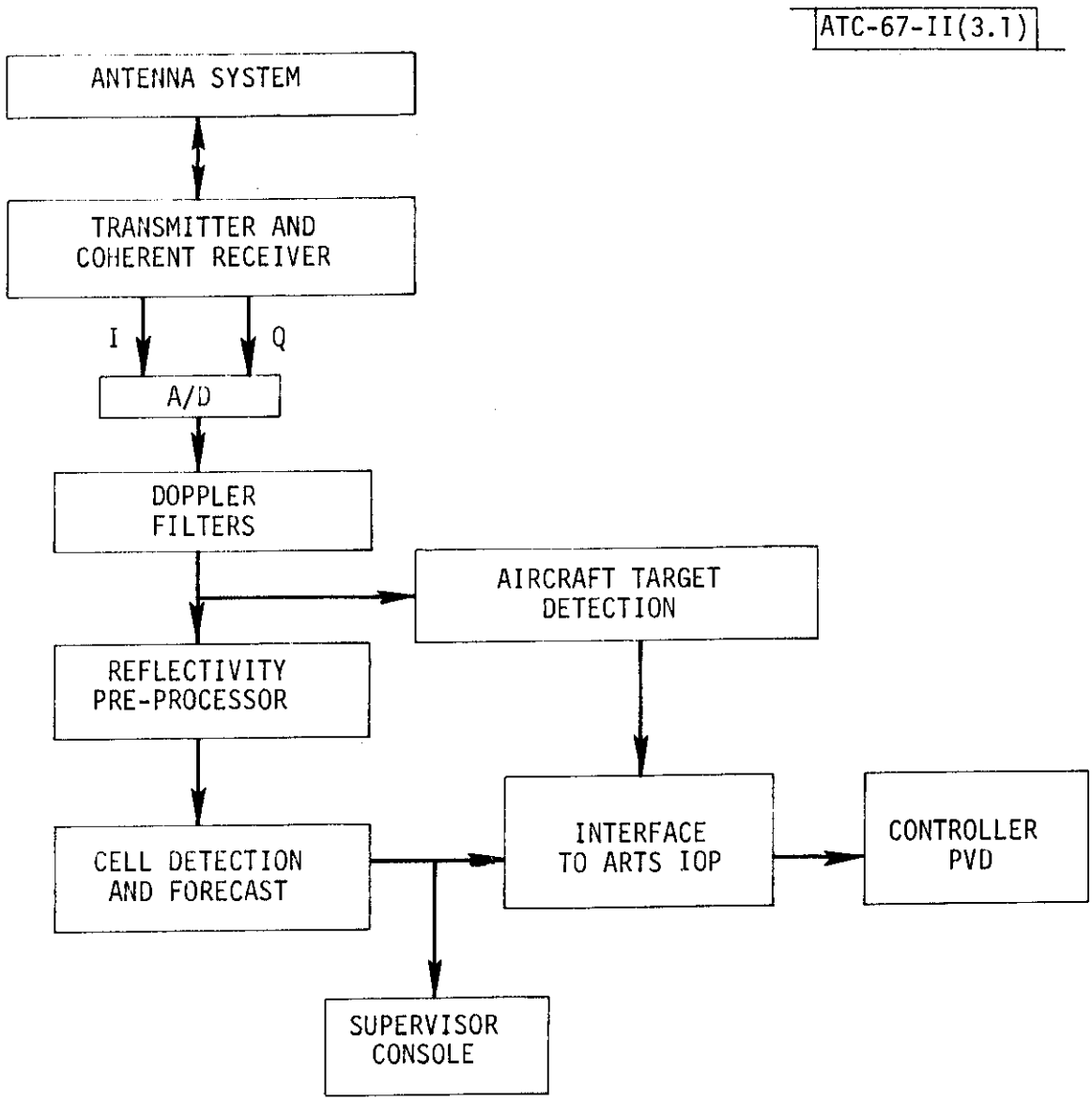


Fig. 3.1 Single RF channel configuration.

The reflectivity preprocessor produces a reflectivity map for the coverage area. The data is then transferred to a mini-computer for execution of the storm cell detection and forecasting algorithms. The resulting cell data is formatted for interfacing with the ARTS IOP and display on the controllers' PVD. The cell data is also displayable on a supervisor's console which is part of the total weather data management system [5].

### 3.2.2 MTD Common Elements

The common signal path for aircraft and weather detection includes the RF and IF stages, A/D conversion of coherent in phase (I) and quadrature (Q) signals, and digital Doppler filtering.

The timing structure of the MTD* is based on a 10 pulse coherent processing interval (CPI) in each 1/16 nm range gate to a maximum operating range of about 48 miles. The PRF in successive CPI's is varied to avoid blind speeds, but this does not impact on weather data. Each CPI is processed through a 3-pulse canceller and 8-point filter algorithms to produce 7 filter outputs corresponding to non-zero Doppler. A zero-velocity output is produced by a low pass filter bypassing the 3-pulse canceller.

The average PRF for the ASR is near 1,200 Hz. At S-band the 3 dB width and spacing of the Doppler filters correspond to approximately 13 knots velocity. (See Appendix B.)

The magnitude of each filter output is computed by an algorithm that approximates $\sqrt{I^2+Q^2}$. The separate weather processing begins with the magnitude outputs.

### 3.2.3 Reflectivity Preprocessor

The functions of the preprocessor are signal averaging, ground clutter elimination and range normalization.

---

*The parameters stated here pertain to the model documented in Ref. 3. A new version currently under development has slightly different parameters, but performs essentially the same functions. The new implementation is based on programmable microprocessors (PMP) which are sufficiently flexible to execute most of the weather preprocessing functions.

Prior to signal combining, the filters should be equalized in gain so that the weather echoes are equally weighted independent of average Doppler offset. Gain equalization can be accomplished through the coefficients in the filter algorithms or by scaling the output magnitudes. The weather echoes, when present, seldom occupy more than three adjacent filters since the weather spectral spread (rms) rarely exceeds 15 knots. Therefore, a significant improvement in weather SNR is attainable by combining only the two or three largest filter outputs which are the most likely to contain weather echoes.

The inclusion of the zero velocity filter requires special consideration. Its output is often dominated by ground clutter and would, in those cases, corrupt the weather reflectivity estimate. However, the zero-velocity filter output cannot simply be discarded. As shown in Appendix B, a substantial fraction, up to 50%, of the weather echoes have velocity that places more than half the energy in the zero velocity notch. The zero velocity filter is to be incorporated in the reflectivity estimate whenever its output is more likely to be weather than ground clutter. This determination is made on the basis of the generally larger Doppler spread of weather echoes which causes more energy to appear in the non-zero filters with weather than with ground clutter.

The spectral spread of the ground clutter is primarily due to antenna beam modulation. The rms spectral width due to this effect is given by [9].

$$\sigma_g = \frac{\alpha\lambda}{10.7\ \theta_2} \text{ m/sec}$$

where for the ASR

$\lambda$ = 0.1m wavelength

$\alpha$ = 75 deg/sec rotational rate of antenna

$\theta_2$ = 1.0 deg two-way half-power beamwidth

Hence $\sigma$ = 0.7 m/sec in contrast to a minimal weather spectral spread of 2 m/sec.

Using the methods of Appendix A we find for a specific filter realization of the MTD that a weather spectrum centered on zero Doppler with a nominal spread of 4 m/sec is attenuated by 14 dB through the first non-zero filter. A ground

clutter spectrum with a spread of 0.7 m/sec is attenuated by 38 dB. Thus a simple test can be made on the filter output magnitudes to decide whether the zero filter contains ground clutter or weather; e.g., if the ratio of the zero filter output to both of the adjacent filters is greater than 18 dB, the zero output is discarded. Otherwise it is combined with the adjacent filter which failed the ratio test provided that filter also has the largest output of the non-zero velocity filters. This example is intended to illustrate the concept; actual parameter settings will depend on more detailed analysis involving filter and weather spectra, signal-to-noise ratio, etc. Of course, if weather and ground clutter echoes of comparable magnitude overlap in range, azimuth and Doppler, reflectivity errors will be incurred.

To properly combine the weather energy from several Doppler filters, the square magnitudes should be summed. This can be accomplished by repeated application of the magnitude algorithm with two inputs (I and Q above). The algorithm is re-entered for each added filter.

After the selected filters have been combined for a particular range gate, the result is one sample of the Rayleigh random process whose mean power (after range normalization) is the desired reflectivity estimate. In Section 2.2 the relationship of estimate fluctuation to the number of independent samples averaged was discussed for linear, square law and log magnitude averaging. Since the result of filter combining is a linear magnitude, it is convenient to deal with magnitude averages. The objective of 0.5 dB precision is attained when about 100 samples are averaged. The samples from different range gates are independent, and 8 successive gates may be summed resulting in a resolution bin size of 0.5 nm or approximately 1 km. In the azimuth dimension one CPI corresponds to one half beamwidth; hence two CPI's, nearly independent samples, may be summed while retaining the required angle resolution. Finally, multiscan averaging in each resolution bin over 6 to 8 rotations will yield a reflectivity map with the desired precision. The map dimensions are 256 azimuth by 90 range bins.

Before this data can be correctly termed a reflectivity map, range normalization must be applied. In Section 3.1.2 it was pointed out that the STC characteristics optimized for aircraft detection introduces weather echo variation dependent on range, R, that should be corrected. With the receiver at full gain and assuming complete beam filling the normalization factor is $R^2$. During STC action the normalization is modified, e.g., for $R^4$ STC the factor is $R^{-2}$ to yield the net $R^2$ behavior. The normalization can be applied additively if the data has been transformed to logarithmic units.

Transformation to logarithms is desirable also for the computer input. This choice minimizes core storage and simplifies the relative reflectivity computations since ratios are expressed as differences of logarithms.

The issues of data representation, word length, etc. are left to detail design. However, it is anticipated that multiscan averaging would be performed by means of a solid state memory external to the mini-computer. The capacity per resolution bin should be sufficient to avoid data truncation before all samples are accumulated. Thereafter, the sum may be rounded to an acceptable number of significant bits. Upon conversion to logarithms 8 bits should suffice for each bin to cover a dynamic range in excess of 60 dB with a resolution of 0.25 dB. Moreover, an 8-bit byte is convenient for data manipulation in a mini-computer. The software algorithms for cell detection, forecasting and display are discussed in Section 3.5.

## 3.3 Dual Channel Configuration Coherent Processing

### 3.3.1 Overall System Structure

A system that permits separate optimization of aircraft and weather detection without compromising the performance of either is diagrammed in Fig. 3.2. In this version the weather channel employs coherent processing and performs functions like those described above for the single channel configuration.

The system permits the option of selecting either linear or circular polarization to optimize aircraft detection depending on weather conditions. An opposite sense circular polarization port is brought out to feed the weather

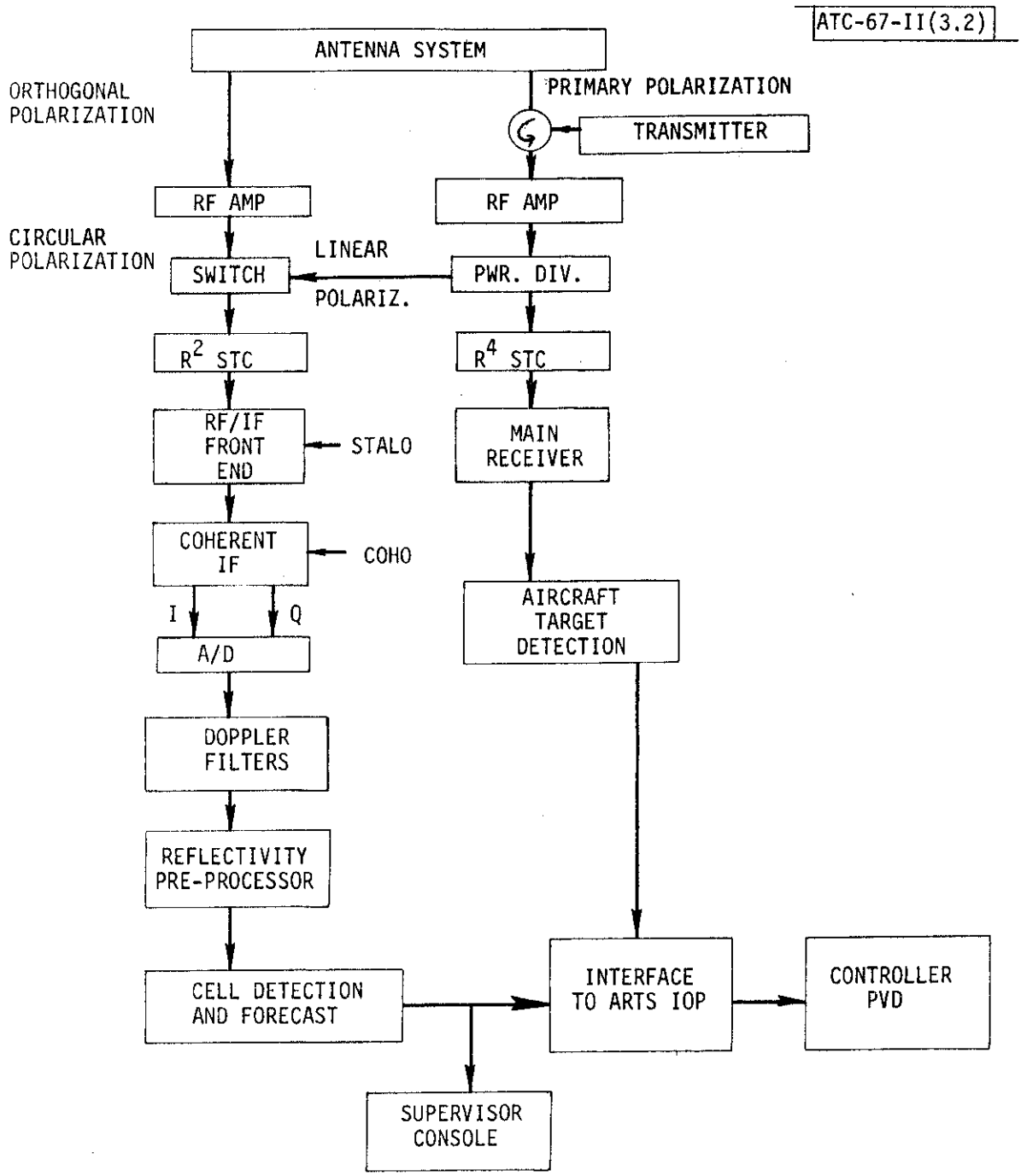


Fig. 3.2 Dual RF channel configuration coherent processing.

channel whenever circular is selected. Since orthogonal linear polarization is not suitable for weather echoes, the primary polarization is switched into the weather channel when linear is selected. The power division and switching takes place after RF amplification and before STC action. Reference frequencies and timing signals for the weather channel are derived from the main transmitter/receiver.

Since the signal paths are not shared between aircraft and weather detection, some latitude exists in the detailed parameters of the weather channel but little advantage can be realized from this flexibility. The pulse width and PRF timing is, of course, common, and the analog receiver components could for convenience be copies of the aircraft channel. The power budget calculation in Section 3.1.2 revealed that the weather receiver channel has adequate margin and could even be degraded somewhat below the main channel.

In an integrated digital system for aircraft and weather, although the data elements are not the same, there is sufficient similarity in processing that common control functions can be implemented for the MTD and reflectivity preprocessor. This would include operations such as memory addressing, timing and parts of computation control.

### 3.3.2 Reflectivity Preprocessor

The preprocessor in the dual channel coherent configuration performs nearly the same functions described in Section 3.2.2 for the single channel system. Without the constraint of utilizing the MTD Doppler filter characteristics, the design of these filters could be modified. For example, fewer filters having wider bandwidth might be satisfactory. This question is best left to a detailed design study, since it is also related to the advantage of shared control structure with MTD.

One step which can be eliminated from the preprocessor under dual channel operation is range normalization. The separate STC for weather echoes can be adjusted to have $R^2$ or similar optimized gain variation.

The preprocessor functions conclude as before with the transfer of the multi-scan reflectivity map to a mini-computer where storm cell tracking and forecasting proceeds as described in Section 3.5.

## 3.4 Dual Channel Configuration Noncoherent Processing

### 3.4.1 Overall System Structure

When aircraft and weather detection follow separate signal paths, the possibility of noncoherent processing in the weather channel should be considered because of potential cost savings relative to a coherent Doppler system. A block diagram of a noncoherent configuration is shown in Fig. 3.3. The dual channel RF and switching arrangement is the same as the one described in Section 3.3.1.

In the conversion from IF to video a logarithmic detector has replaced the coherent (I,Q) detectors. With the proper STC the dynamic range of the log detector need be no greater than 60 dB. An A/D converter with 8 bit accuracy can adequately quantize the log variable to less than 0.25 dB resolution.

The reflectivity preprocessor receives the digitized video and a second input resulting from a test based on Doppler spread to distinguish non-overlapping weather and ground clutter. Multiscan signal averaging is followed as in the previous configurations by transfer of the reflectivity map to a mini-computer for cell detection, forecast and display.

### 3.4.2 Reflectivity Preprocessor

The averaging of N logarithmic samples is one of the methods for estimating the mean reflectivity, $\overline{A^2}$. Section 2.2 reviewed the pertinent statistics, viz. the mean log is 10 log $\overline{A^2}$ - 2.5 (dB) and the standard deviation is $5.57/\sqrt{N}$ (dB). The desired 0.5 dB precision is obtained by averaging 128 independent samples represented by 8 range gates, 2 half-beamwidths, and 8 scans.

Since the noncoherent weather processor has few features in common with aircraft detection there is no strong motivation to retain the range-gate timing of the MTD. An A/D sampling rate of 1.2 MHz is adequate and leads to 1 km resolution when 8 range gates are combined.

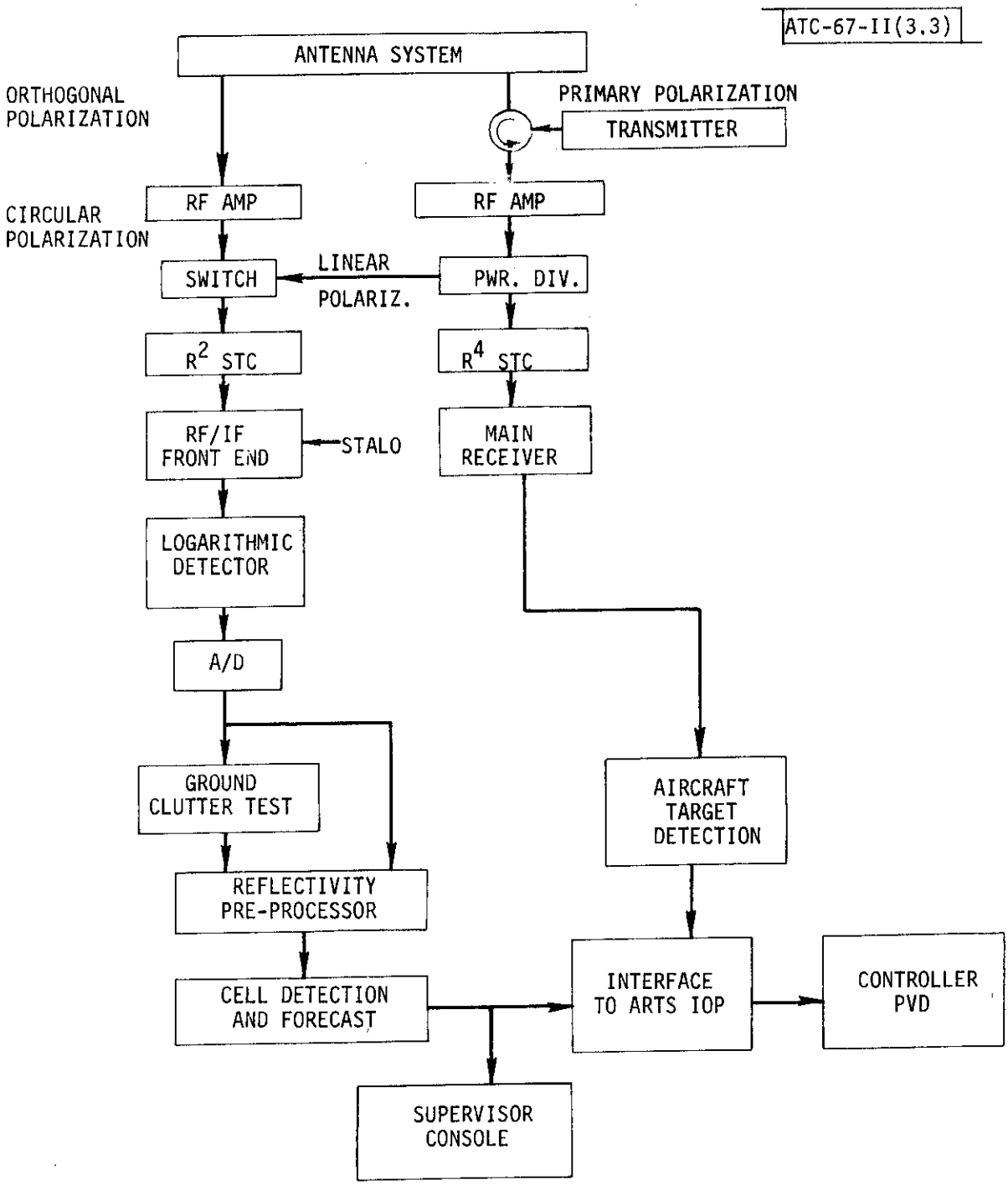


Fig. 3.3 Dual RF channel configuration noncoherent processor.

In the coherent systems the average radial Doppler of the rain is a discriminant to extract weather echoes even when there is overlapping ground clutter. The analysis in Appendix B showed that this procedure is successful in about 50% of the overlap situations for typical translational velocities of storms. For the cases of small radial velocities, a Doppler spectral spread criterion is used to eliminate obvious ground clutter from the reflectivity estimate. A noncoherent processor is insensitive to average radial velocity and is forced to treat all echoes as having zero Doppler offset. However, a Doppler spread criterion is still applicable since the spectral width is evidenced by pulse-to-pulse envelope fluctuations.

The rms spectrum width due to antenna beam modulation alone was found to be equivalent to 0.7 m/sec. By comparison, the standard deviation of the precipitation spectrum goes from 1.0 to 10 m/sec depending on the degree of turbulence and shear conditions. The larger weather Doppler spread opens the possibility of classifying echoes as being either ground clutter or weather.* The categorization is accomplished with the aid of a high pass filter acting on the signal envelope. Although the spectral shapes are distorted by passage through a log detector, a spectral width criterion is still applicable.

The accumulation of video samples from each range gate proceeds under the control of a ground clutter test as follows. The absolute value of the high pass filter output is a measure of the signal strength that has passed through the filter and is to be compared to the total signal bypassing the filter. If the filter output is less than a predetermined fraction of the total signal, the spectral spread is small, the echo is assumed to be primarily ground clutter, and the video output is inhibited. If the converse is true, the Doppler spread is sufficiently great that the echo is assumed to be from rain. Although the classification may not be correct in all cases, a large portion of strong ground clutter can be eliminated. Some ground clutter patches overlapped by rain echoes may be accepted initially as weather, but would be rejected as storm cells by the tracking algorithm for lack of spatial movement.

*A third category denoted "uncertain" was also considered to account for situations where the binary classification is not clearly evident. However, the complication of carrying the extra category identification through most of the processing steps does not appear justifiable.

Storm cells that overlap extended ground clutter regions would have a reduced probability of detection or erroneous reflectivity estimate.

The design details of the high pass filter having a cut-on frequency near 1 m/sec need further investigation. Its form depends in part on the PRF timing. With a four-pulse stagger as in the ASR(8), a strictly periodic sampling train can be produced by a simple sum of four successive sweeps. The resulting sequence, at one fourth the original average PRF, is suitable as an input to a recursive filter. With a multiple burst PRF, such as in the MTD, the filter design is less obvious. A recursive type filter would have to re-initialize each PRF interval. Alternatively, a finite impulse response filter for the constant PRF interval can be designed to approximate the desired response.

The reflectivity map formed by summing the selected logarithmic samples is formatted for transfer to the mini-computer by simply rounding the sum to 8 bits.

The noncoherent weather processor could be considered as a retrofit for radar systems where the cost of a coherent implementation is excessive. The cost advantage must be weighed against the reduced effectiveness in ground clutter discrimination.

### 3.5 Cell Detection, Forecasting and Display

For all the candidate systems described above, the output, consisting of a reflectivity map for the coverage area, is transferred to a mini-computer system where the data is further processed to generate the storm cell structure and forecast of future positions for display to ATC controllers.

The details of the cell detection, tracking and prediction algorithms are covered in Reference 2. The procedure begins with a search for local reflectivity peaks which are indicative of storm cells. For each peak a contour down by a selected fraction from the peak is found. Contours surrounding more than one peak are discarded. A storm cell is characterized by its peak intensity, the area of the surrounding contour, and the location of the peak or

another measure of contour center. The cell data from successive acquisition cycles is passed on to a tracker where cell trajectories are determined. Based on the track history, a projection to a specified time in the future can be made. Also at this point in the procedure, stationary cells representing ground clutter are discarded. The cell attributes including intensity, size, growth or decay are used to assess the cell severity before the data is conveyed to the display processor.

The normal display consists of the cell position and attributes as projected to current time at the control facility. At the option of the operator, the view of current conditions may be replaced by a forecast for selected time intervals up to 20 minutes into the future.

In the TRACON facilities the weather situation is ultimately depicted on the controllers' PVD and a supervisor's console. This data flow would be integrated into the recommended weather data management system, specifically, the TRACON WEather Processor (TWEP) described in Reference 5. TWEP acts as an interface between the radar processor and the ARTS IOP which displays data on the PVD's. This link could exist without TWEP if appropriate functions are included in the radar mini-computer. Since the weather data originates at the same radar as the aircraft reports, a common data channel for weather and surveillance data could be implemented.

# 4.0 INTERIM MTD WEATHER EXTRACTION

## 4.1 Requirements for Weather in all Digital ARTS Display

As part of the ARTS enhancement program the FAA is sponsoring the development of an all digital display system. Digitized target reports from beacon and/or radar reply processors constitute the input to the system. Since analog radar video is not displayed, a vector generator capability is planned to depict weather echo contours and map outlines.

If the all-digital system including the MTD is deployed before the storm cell detection and forecasting procedures described elsewhere are developed, useful but limited weather data in the form of fixed reflectivity contours can be extracted as an interim measure. These data extraction and display methods would not satisfy the real needs of controllers for hazardous turbulence depiction and forecasts. However, the early deployment of MTD and the all-digital system demands that provisions be made to furnish the controllers with radar weather data. The data should be equivalent to or better than what is currently available from the ASR in analog form or from the ARSR narrowband weather subsystem.

The following sections describe the recommended methods for extracting weather data from the MTD in a relatively simple manner to generate fixed reflectivity contours for the controller display. The flexibility of the MTD opens the possibility of signal processing prior to data transfer to the ARTS IOP that can improve overall system operation.

## 4.2 Recommended Processing

The recommended procedures follow those of the single RF channel configuration in Section 3.2 up to the point before the reflectivity map is found by multiscan averaging.

### 4.2.1 Selective Summation of Filter Outputs

The natural beginning of the separate processing for weather extraction is with the output magnitudes of the 8 Doppler filters. It is assumed the

filters have been normalized for equal gain. The weather echoes will in general be significant in no more than three adjacent filters since the filter width and spacing is about 13 knots and weather spectral rms width rarely exceeds 20 knots. The desired weather processing consists of summing the square magnitudes of those filters whose outputs are predominantly weather as compared to noise or ground clutter.* For the non-zero Doppler filters a subset, say 2 or 3, containing the largest signals is summed, thereby yielding an improvement in SNR over the receiver input. Improved SNR partly mitigates the effect of STC on weather data (see Section 3.1.2).

The zero-velocity filter is summed if its output is more likely to be weather rather than ground clutter as determined by the amount of Doppler spectral spread. The algorithm described in Section 3.2.3 is employed here also viz. the zero filter is added if the ratio of its output to either of the adjacent ones is below a preset limit. This processing step is necessary to avoid loosing a significant fraction of weather echoes (see App. B).

The accumulation of square magnitudes may be accomplished by entering the two input magnitude routine once for each added component, i.e.,

$$\sqrt{F_1^2 + F_2^2 + F_3^2} = \sqrt{\left(\sqrt{F_1^2 + F_2^2}\right)^2 + F_3^2}$$

where $F_i$ represents a filter output magnitude.

After the root-sum-square magnitude has been computed, the results are accumulated over 16 range gates and 2 coherent processing intervals. The range resolution is 1 nm, a factor of two coarser than the system discussed in Section 3.2. Without multiscan averaging, the number of independent samples summed is 32 giving a precision of 0.8 dB at large SNR. Since the interim solution is not intended to support individual storm cell detection, but rather to provide weather contours, the larger spatial and amplitude resolution is acceptable.

*Aircraft targets that appear as weather may be removed in later processing stages.

### 4.2.2 Range Normalization to Compensate for STC

The physical quantity of interest for radar weather is the volume reflectivity or a related measure, the reflectivity factor. When the receiver gain is held constant and under the assumption that the scattering volume completely fills the antenna beam, the conversion from signal strength to reflectivity involves normalization by the square of range ($R^2$). In a receiver with STC the conversion to reflectivity must take account of the range dependent gain variation. If the STC has an $R^2$ characteristic out to the maximum useful operating range, no further conversion is necessary. Correction is required with radars intended for point targets which employ $R^4$ STC out to a preset distance from the radar.

The range normalization for weather data should be adapted to the STC characteristics in use. This computation can be mechanized in a number of ways depending on specific implementations of the MTD. The normalization numbers can be stored in a small memory. The addressing procedure or the contents of the memory are established at the time of site adaption and selection of STC characteristics. Range normalizations other than simple integer powers of R can also be accommodated based on a more detailed optimization involving antenna elevation pattern, assumed storm height and STC. A procedure for deriving such a range normalization is outlined in Appendix C.

### 4.2.3 Hardware Thresholding

The data from the MTD is to be used for finding contours of fixed reflectivity level and displaying these via a vector generator on the PVD. Thresholding the data in the MTD at the desired levels can facilitate this objective and at the same time reduce the rate of data transfer to the ARTS IOP. Instead of transferring a reflectivity value for each resolution bin and forming contours in software, the up and down threshold crossings for each selected level are determined for each azimuth bin (2 CPI's). The ranges at which the

crossings occur are transferred to the software along with the azimuth identifier.* This data is sufficient to generate contours by connecting the appropriate points. However, since the number of points on the contour may exceed the capacity of the display's vector generator, a software algorithm can be used to replace the point-by-point contour by "best-fit" line segments.

*The narrow-band weather subsystem (formerly WFMU) employs this concept in extracting weather from the ARSR.

## 5.0 A LONG RANGE WEATHER RADAR TO SUPPORT FAA, NWS AND AWS

### 5.1 Overall System Structure

A joint use network of weather radars to serve all interested government agencies promises significant cost savings to each user agency. This chapter covers the characteristics of a weather radar that satisfies the ATC requirements outlined in Chapter 2 and has the potential of providing anticipated data inputs to other users.

The geographic structure consists of a weather radar and on-site processor connected by data link to several user facilities. The distribution of processing functions between radar site and other facilities is governed by the communications load and by the advantages of centralized processing. The NWS functions incorporated in the Radar Data Processor (RADAP) are candidates for on-site processing. Some adjustments of parameters and mode of operation may be necessary to make the RADAP functions compatible with the ATC requirements. For the ATC weather support, the on-site processing comprises the storm cell detection and determination of cell attributes such as intensity, area and height. The cell description and contour data for perhaps two fixed reflectivity levels are transmitted to an ARTCC WEather Processor (AWEP) [5]. AWEP combines data from radars with overlapping coverage, generates the very short term forecast and interfaces with the controller and supervisor displays.

The on-site equipment consists of a pencil beam radar automatically sequenced through a data acquisition cycle under the control of the on-site mini-computer. The radar employs coherent Doppler processing for ground clutter suppression and for the benefit of meteorologists who wish to analyze and interpret radial wind fields. The Doppler data is extracted by means of a pulse-pair correlator.

An overall block diagram of the system configuration is given in Fig. 5.1.

### 5.2 Preliminary Inputs from AWS ROC

Specific requirements for next generation AWS and NWS weather radars are not fully formulated. A preliminary draft of the Required Operating Characteristics (ROC) prepared by the Air Force states features such as unattended

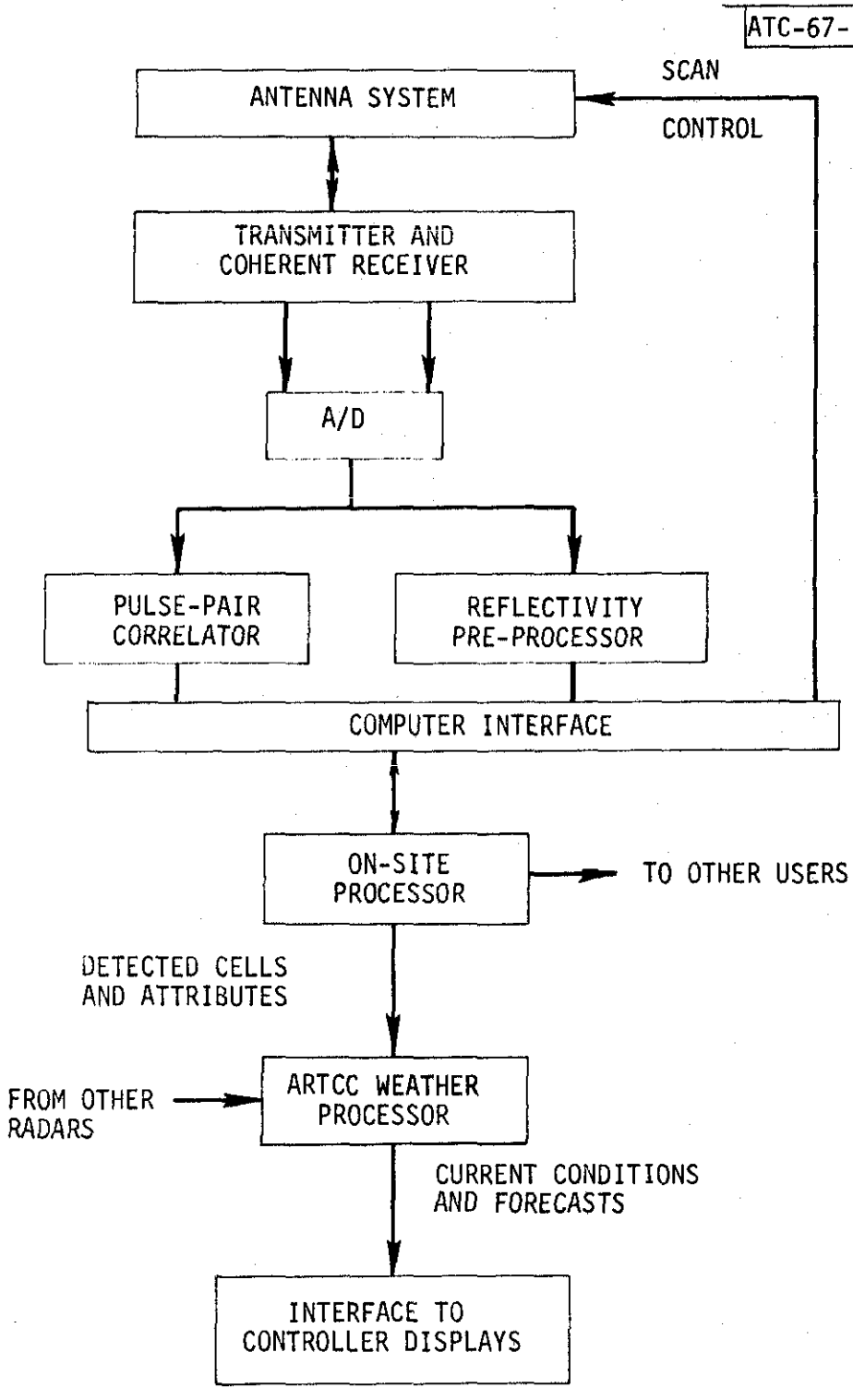


Fig. 5.1 Weather radar for ATC and other users.

operation, digital output data, Doppler capability and automatic severe weather alerting. Many of the functions are in the category of data processing and communication which are outside the scope of the basic sensor. However, the ROC does include a specification of reliable measurements out to 110 km plus detectability of minimum 13 dBZ precipitation at 400 km. The latter is well beyond the approximately 200 km maximum useful range of the radar for ATC weather purposes.* If the density of radars is sufficient to provide full coverage for ATC, the 400 km operating range would be unnecessary. The requirement primarily impacts the receiver dynamic range and the selection of PRF, and, of course, demands the added capacity to handle the data. Because of the significant implementation impact, the long-range, low reflectivity requirements need strong justification. The following sections go into more detail on the choice of radar parameters.

## 5.3 Recommended Radar Parameters

### 5.3.1 Carrier Frequency

The choice of RF frequency is governed by the following issues:

a) angular resolution

b) attenuation in rain

c) reflectivity

d) antenna gain

e) Doppler sensitivity

The candidate frequencies are S-band ($\lambda$ = 10 cm) and C-band ($\lambda$ = 5.3 cm). Higher frequencies have excessive attenuation in rain, and lower frequencies lead to insufficient angular resolution.

To achieve a beamwidth of 1° as stated in the requirements (Section 2.6), the ratio of antenna diameter D to wavelength $\lambda$ should be $D/\lambda = 70$. This

*For purposes of this preliminary design exercise, 200 km instead of 180 km will be used for the ATC operating range.

assumes a circular aperture illumination of the form $0.25 + (1-r^2)^2$. The corresponding antenna diameters are 7 m(23.2 ft) and 3.7 m(12.3 ft) for S-band and C-band, respectively.

Attenuation in rain has been related to reflectivity factor Z by (1)

$$k_p(\text{dB/km}) = Z^{0.62} \begin{cases} \times 0.3 \times 10^{-4} & \text{S-band} \\ \times 1.12 \times 10^{-4} & \text{C-band} \end{cases}$$

for 10 log Z = 50 dBz, about 50 mm/hr rainfall, the attenuation is 0.038 and 0.14 dB/km. The consequence of attenuation along the path to the target storm cell is primarily an underestimation of its intensity. This effect can be corrected by a bootstrap method of integrating the attenuation along the path using the reflectivity data itself. Due to the accumulation of errors with the method, successful correction depends on high accuracy in the data. However, with or without correction, the shape and location of storm cells are affected only to the extent that there exist strong azimuthal gradients in attenuation errors. This is unlikely to happen except where small intense cells intervene between the radar and larger weak cells.

Items (c) reflectivity and (d) antenna gain affect the system power budget. C-band is preferred but the issue is of secondary importance in frequency selection.

The final issue on Doppler concerns the maximum unambiguous estimates of velocity for a given PRF. The relation $f_d = 2\ v/\lambda$, where $f_d$ is Doppler shift, and v is target speed, favors longer wavelengths to accommodate larger v for $|f_d| < 1/2$ PRF. As will be seen below the PRF constraints are such that pulse stagger is required in any case. By employing pulse-pair correlation with pulse-stagger, accurate, unambiguous Doppler estimates are attainable at either S-band or C-band.

The dominant factor in frequency selection is the antenna size for the specified beamwidth. A 23 ft parabolic dish leads to a mechanically difficult

implementation for the antenna itself, the mount, and radome. For a network of many radars the smaller dimensions and corresponding lower costs offered at C-band are much more attractive.

The other factors in the frequency choice either favor C-band (c and d) or are amenable to solutions other than lowering the frequency. We conclude that C-band should be the operating frequency of the new weather radar.

### 5.3.2 Pulse-Pair Correlation

The method of Doppler measurement known as pulse-pair correlation has received much attention in the literature and is favored for weather radar applications [11]. This is considered a minimum capability for a new network of operational weather radars. We have not tried to anticipate more sophisticated Doppler processors for weather that may be evolved in the future.

The complex correlation of pairs of successive pulses in each range gate is computed as

$$\hat{R}(\tau_s) = \frac{1}{N} \sum_{n=1}^{N} s(nT)\, s^*(nT + \tau_s)$$

Here $s(t)$ is a complex video process, $\tau_s$ is the delay between pulses in a pair, and N products of pairs separated by T are averaged. From the complex correlation $\hat{R}(\tau_s)$ the mean frequency is estimated as:

$$\hat{f} = \frac{1}{2\pi\tau_s} \operatorname{Arg}[\hat{R}(T_s)]$$

This estimator can be derived from maximum likelihood theory. Its reasonableness is seen from the Fourier transform relation between power spectrum, $S(f)$, and correlation function $\rho(\tau)$, and the translation property of the transform, i.e., letting "$\Leftrightarrow$" indicate transform,

$$\text{if} \quad S(f) \Leftrightarrow \rho(\tau)$$

$$\text{then} \quad S(f+f_o) \Leftrightarrow e^{j2\pi f_o \tau} \rho(\tau) = R(\tau)$$

The correlation $\hat{R}(\tau_s)$ is also the basis for an estimator of the spectral variance. Its properties are discussed in the literature, [4,8] but the estimate has found little practical application.

The spectral variance defined by

$$b_1 = \frac{\int f^2 S(f)\, df}{\int S(f)\, df}$$

plays a role in determining the statistical quality of the mean frequency estimator.

Reference 8 finds the standard deviation of $\hat{f}$ to be

$$\sigma_{\hat{f}} = \frac{b_1 \Phi}{\sqrt{N}}$$

where $\Phi$ is a normalized standard deviation dependent on SNR and the parameters $b_1\tau_s$. Figure 5.2 is a plot of $\Phi$ vs. $x = 2\pi b_1 \tau_s$. The optimum x is near one and values larger than two should be avoided.

These considerations set a limit on the useful interpulse period $\tau_s$. A nominal value for the spectral spread of $b_1$ is 4 m/s or 150 Hz at C-band. Hence for $x < 2$, $\tau_s < 1/(150\pi) = 2.1$ ms. Assuming N = 18 pairs and $\Phi = 2$, the resulting estimate error is $\sigma_{\hat{f}} = 71$ Hz = 1.9 m/s.

5.3.3 Pulse Stagger Intervals

The 400 km range objective of Sec. 5.2 demands a pulse interval of at least 2.67 ms. According to the preceding analysis, this spacing is unacceptable for Doppler estimation because of excessive error. One is, therefore, led to consider staggered pulse intervals where one spacing allows the maximum range coverage for reflectivity only and other shorter intervals are suitable for mean frequency estimation.

In addition to the mean frequency error, one must consider the unambiguous interval of the estimate. Assume one pulse pair is separated by 1.33 ms corresponding to the 200 km operating range for ATC. The unambiguous Doppler

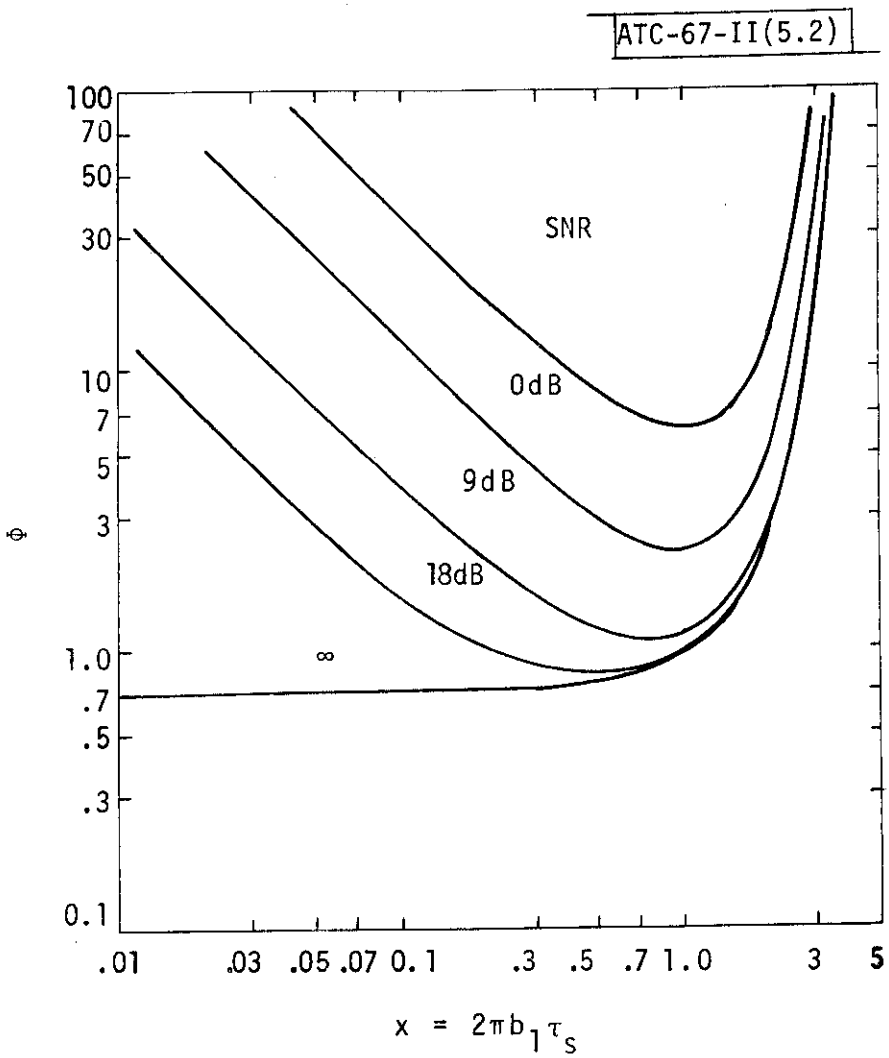


Fig. 5.2 Normalized standard deviation of mean-frequency estimator versus pulse-pair spacing. [8]

interval of ±375 Hz or ±10 m/s is too small for observing storm motion. This limitation can be overcome by employing two different pulse intervals for mean frequency estimation and combining the results to produce an unambiguous answer.*

A possible 3 pulse stagger sequence is [3.06, 1.7, 1.36] (ms). The long interval serves for maximum range detection. The 5:4 stagger ratio of the other two periods leads to an unambiguous Doppler interval of

$$\frac{5}{1.7} = \frac{4}{1.36} = 2.94 \text{ kHz}$$

corresponding to ±39 m/s or ±76 knots which is adequate for analyzing wind fields.

For illustration, the sum of the two shorter intervals was arbitrarily set to equal the longest interval. The stagger sequence parameters actually represent degrees of freedom that can be used to optimize the design of a multiple canceller to reject ground clutter. A pulse canceller is one realization of a high pass filter for separating weather and ground clutter on the basis of average radial Doppler.

5.3.4 Independent Sample Size Factors

From Section 2.2 we recall that 83 independent samples of linear video must be averaged to attain 0.5 dB rms precision. If the pulse repetition interval is less than the decorrelation time of the random process, more samples are required. For purposes of counting samples, the pulse separating the two short intervals in the stagger sequence may be ignored. The precipitation echo intensity is strongly correlated for delays as short as 1.7 ms; hence the pulse provides little non-redundant information. The effective PRI

*At S-band the 200 km PRI produces a Doppler interval of ±19 m/s or ±37 knots which is still too small. A reduction of the PRI to avoid staggered pulse-pair correlation would unduly restrict the range of utility of the radar for wind field analyses.

may, therefore, be taken as 3 ms, and N pulses at this spacing are averaged. Assuming a low spectrum spread due to turbulence of 0.7 m/s, the equivalent number of independent samples $N_{eq}$ = N/3.5 [see Appendix C]. For $N_{eq}$ = 83, N = 290 pulses.

Excluding the possibility of frequency diversity, the necessary number of pulses may be collected in range and azimuth. In range the 1 km resolution bin may be subdivided into several range gates, with a corresponding adjustment in pulse width to achieve independence between adjacent gates. The limitation here is primarily the computation and storage burden imposed on the processor by small range gates.

In azimuth, the available number of pulses in a 1° beam width is a function of scan rate. If data acquisition speed were not a problem, the antenna could simply be rotated slowly so that a sufficient number of pulses is collected in each range gate. However, as indicated in Section 2.4, the data acquisition cycle, including elevation scans (see Section 5.7), should be completed in 2 to 3 minutes.

A feasible compromise among the above considerations consists of the following: rotation at 1.5 rpm or 111 ms/deg., implying 37 pulses per 1° resolution bin; combining 8 range gates spaced at 1/8 km (0.833 μsec) for a total of 296 pulses.

### 5.3.5 Power Budget

Several of the remaining radar parameters appear in the system power budget and will be treated in that context. The power budget is predicated on achieving an SNR per pulse of 10 dB for 25 dBZ reflectivity factor at 200 km. The parameters listed in Table 5.1 are all reasonable and can be achieved without difficulty.

Pursuing the AWS requirement (Section 5.2), to observe low reflectivity (13 dBZ) targets at 400 km, a 18 dB difference must be accounted for. The possible mechanisms for extending the range include 1) relax the SNR requirement, 2) increase transmitter power, and 3) reduce noise figure.

TABLE 5.1

C-BAND REFLECTIVITY POWER BUDGET

$$\overline{P_r} = \frac{\pi^3 P_t G^2 \theta\phi\, h}{1024\, \lambda^2 \ln 2} \frac{|K|^2}{r^2} Z \quad \text{(Battan [1], p. 42)}$$

| | | | |
|---|---|---|---|
| $\pi^3/(1024 \ln 2)$ | = | 0.0437 | -13.6 dB |
| Transmitter Power, $P_t$ | = | 140 kw | 81.5 dB mW |
| Gain, $G^2 = \eta^2(\pi D/\lambda)^4$ | = | $0.25\ (70\pi)^4$ | 87.0 dB |
| Az beam, $\theta$ = 1° | = | 0.017 rad | -17.6 dB rad |
| El beam, $\phi$ = 1° | = | 0.017 rad | -17.6 dB rad |
| Pulse length, h(0.833 μs) | = | 250 m | 24.0 dB m |
| Wavelength, $\lambda^{-2}$ | = | $(0.053\ m)^{-2}$ | 25.5 dB $m^{-2}$ |
| Maximum Range, $r^{-2}$ | = | $(200{,}000\ m)^{-2}$ | -106.0 dB $m^{-2}$ |
| Constant,* $\|K\|^2$ | = | $(.935)^2$ | -1.2 dB |
| Reflectivity, Z (25 dBZ $mm^6/m^{-3}$) | | | -155 dB $m^3$ |
| Losses | | | -3 dB |
| Receiver Power, $\overline{P_r}$ | | | -96 dB mW |
| Ref Noise Density, $kT_o$ | | | -114 dB mW $(MHz)^{-1}$ |
| Bandwidth, B = 1.6 MHz | | | 2 dB MHz |
| Noise Figure | | | 6 dB |
| | | | -106 dB mW |
| SNR per Pulse at Maximum Range | | | 10 dB |

*Related to the index of refraction. See Reference 1.

If the entire 18 dB differential is absorbed by SNR, the SNR per pulse becomes -8 dB, which is unsatisfactory for reflectivity estimation. Moreover, all three approaches increase the requirements of the receiver and A/D converter to accommodate a wide dynamic range. As discussed in the succeeding subsection, adequate dynamic range is difficult to achieve even without the low reflectivity objective. The need for observing low precipitation echoes at long ranges should, therefore, be thoroughly justified.

## 5.4 RF/IF Components and A/D Converters

No significant departures from conventional design are required in the RF/IF stages of the radar. Only the receiver dynamic range needs special attention. Front-end STC is expected to compensate for 40 dB of $R^2$ echo dependence from 2 to 200 km. The remaining variation of 55 dB from noise floor to peak reflectivity must be accommodated by the coherent detector and A/D converters. Extrapolating from the 45 dB dynamic range achieved with the first MTD developed at MIT Lincoln Laboratory, the desired performance may be achievable with normal advances of the state of the art in components and signal processing. If not, some degradation at the extremes of the dynamic range would have to be tolerated.

For operation out to the 400 km, it should be noted that the front-end $R^2$ STC terminates at 200 km. The receiver is at full gain for targets beyond that distance, and subsequent range correction should be applied to the reflectivity estimates. This can be accomplished by an $R^2$ gain control in the IF or video. In contrast to front-end STC, this gain has no effect on SNR, but it serves to maintain the signals in the favorable operating region of the A/D as the SNR degrades.

## 5.5 Reflectivity Preprocessor

The reflectivity preprocessor for the weather radar consists of those computational elements that accept digitized I and Q video and produce a reflectivity map for a spatial sector.

### 5.5.1 Ground Clutter Suppression

The Doppler capability of the radar, although not a direct part of storm cell tracking, is useful in the discrimination of ground clutter and weather on the basis of average radial velocity. An important characteristic of the ground clutter is its rms spectral width $\sigma_g$ due to antenna beam motion. For the parameters of this radar; viz. $\lambda$ = 0.053 m, $\theta_2$ = 0.75° (two way half-power beamwidth) and $\alpha$ = 9 deg/sec (1.5 rpm rotation rate) one has

$$\sigma_g = \frac{\alpha\lambda}{10.7\ \theta_2} = 0.06 \text{ m/sec}$$

The ground clutter spectrum is sufficiently narrow so that a narrow-band zero-velocity notch to reject it would eliminate a negligible portion of the weather. A notch width of ±0.5 m/sec at the 3 dB point should provide adequate suppression of ground clutter. According to Appendix A, when $v_r$ = 0.5 m/sec, a translation speed $v_w$ as low as 2 m/sec is sufficient to ensure over 84% success in extracting accurate weather data. For more typical speeds of 8 m/s (15.5 knots) the success rate is 96%.

The high-pass filter is preferably based on a multiple delay canceller employing an optimized stagger sequence. As an alternative or supplement to the canceller, a recursive realization using a periodic subsequence could be considered.

If necessary, the elimination of even a small percentage of weather echoes by a zero-velocity notch can be avoided by performing a Doppler spread test. Echoes having low average radial velocity but large spread would be processed via a signal path that by-passes the notch filter. Such a test would involve additional computations, perhaps drawing on the mean frequency and variance estimates from the pulse-pair correlator.

### 5.5.2 Sample Averaging

The high-pass filter operates on the I and Q channels in each 1/8 km range gate. Subsequently, the magnitude $\sqrt{I^2 + Q^2}$ is formed, and

samples from 8 range gates and the number of sweeps between 1° azimuth increments are accumulated.

The reflectivity data quantized to no more than 8 bits (logarithmic) per bin is transferred to the on-site mini-computer for further processing or distribution to users.

## 5.6 Pulse-Pair Correlator

The operations performed by the pulse-pair correlator are complex multiplication and averaging. For each of the two smaller stagger spacings $T_i$ the products

$$[I(t) - jQ(t)]\,[I(T + T_i) + jQ(t + T_i)] \quad i = 1,2$$

are formed. The real and imaginary parts of the product are averaged over a sequence of pairs encompassing the 1° beamwidth. For the representative set of parameters offered in Sections 5.3.3 and 5.3.4 the number of pulse-pairs in a beamwidth is given by

$$\frac{111 \text{ ms/deg}}{6 \text{ ms/stagger cycle}} = 18$$

The data may be further averaged over a number of range gates consistent with the desired range resolution.

The extraction of the mean-frequency and spectral spread estimates may be carried out by software after transfer of the data to the on-site mini-computer or by a dedicated hardware processor. The operations consist of

$$f_i = \frac{1}{2\pi T_i} \tan^{-1} \frac{\text{Im } \hat{R}(T_i)}{\text{Re } \hat{R}(T_i)}$$

$$\hat{\sigma} = \frac{1}{\pi T_i} \sqrt{1 - |\hat{R}_i(T_i)| / R_i(0)}$$

The $f_i$ estimates are then further manipulated for ambiguity resolution. Assuming a 1 km range resolution, the time allotted per resolution bin is

$$\frac{111 \text{ ms/az bin}}{200 \text{ range bins}} = 555 \ \mu s$$

Further investigation is necessary to assess the computational load imposed by these operations and to decide how to implement them. Experience with existing pulse-pair correlators will provide useful guidance on this effort.

## 5.7 Elevation Scans

The height information required for ATC and meteorological analysis is to be obtained by a regular sequence of elevation tilt scans. Because of the stringent requirements on update interval for cell tracking, manual probing of storms in the vertical direction is not feasible. In order to minimize the data acquisition period, both the number of elevation tilt scans and the time per scan should be minimized.

The elevation tilt positions need not be uniformly spaced throughout the range of interest. The height requirements can be satisfied by ensuring a vertical sample spacing of less than 2 km up to 9 km. Table 5.6 gives a sequence of tilt angles that meets this condition from 18 km outward in range to a point where 2 km height fails to fill the 1° beam. Each entry in the table represents the upper beam edge, e.g., the 14° tilt covers a 1° sector between 13° and 14°. The 1° tilt is the lowest elevation scan having its lower beam edge on the horizon.

TABLE 5.6

ELEVATION TILT POSITIONS

| | | |
|---|---|---|
| 1° | 5° | 14° |
| 2° | 6.5° | 18.5° |
| 3° | 8.5° | 24° |
| 4° | 11° | 30° |

It is expected that this or a similar sequence of elevation tilts would be satisfactory for all users.

The cell detection process is initiated with the data acquired on the lowest elevation scan. The data from tilt scans is associated with the cells found on the lowest scan to determine the maximum vertical extent of each cell. In forming the association, the requirements on precision can be relaxed from the 0.5 dB value specified for cell detection. This permits a faster scan rate on the elevation tilt scans since fewer independent samples per beamwidth are needed; two to four times faster rotation rate is tolerable.

At the recommended scan rate of 1.5 rpm, the lowest elevation scan consumes 40 seconds. Taking advantage of the maximum scan rate increase for elevation tilt, allows 10 sec. for each of 11 tilts for a total of 150 sec. This is less than the 3 minutes allotted to acquisition in Section 2.4.

## 5.8 Cell Detection

Details of the cell detection algorithm are described elsewhere [2]; here we are concerned with the storage, and data compaction issues.

The total number of resolution bins is 200 (range) x 360 (azimuth) = 72000. With 8 bits per bin this represents 72K bytes of memory in a 16 bit byte-addressable machine, larger than the addressable space without memory mapping. The potential difficulties of processing on such a large data base can be overcome by performing the initial portions of the algorithms "on the fly."

Because storm cells are defined by contours relative to local maxima, sufficient data must be stored to correctly identify the peak and its

surrounding contour. Maximum storm cell dimensions dictate the size of the azimuth sector as a function of range that must be saved before cell contouring begins. Near the radar a 360° sector is needed since cell contours may surround the site. At long ranges a few 1° azimuth bins may suffice.

Detected cells are represented by their locations (center of mass or peak), area, and peak intensity. By association of data from elevation tilt scans the vertical extent of the cell is determined and added to its list of attributes. The cell characteristics in this compacted form are transmitted from the on-site processor to one or more of the ARTCC Weather Processors (AWEP). The delay incurred in transferring this data can be minimized by sending the basic attributes as soon as available during or after the lowest elevation scan. The height data can be transmitted later with a cell identifier, after the necessary number of elevation scans to determine the cell top are completed.

## 5.9 AWEP Radar Functions

The role of AWEP in the weather subsystem for ATC is described in detail in Reference 5. In addition to its weather data management functions, AWEP continues the radar processing by 1) combining data from sensors with overlapping coverage, 2) executing cell forecasting algorithms, and 3) formatting data for interface to controller displays.

The so-called radar netting job assures that the controller is presented with a consistent, meaningful display even when data arrives from two or more weather radars. Also, a cross-calibration check can be performed to verify performance.

The very short range forecast of storm cell movement, growth and decay is produced in AWEP based on the time history of individual cells and clusters of cells. The height information aids in the classification of cell severity and permits storm overflight. To compensate for acquisition and processing delays, the forecast is used to generate the image of "current conditions" at the time the data is displayed to controllers. At the operator's option the

current weather situation is replaced by a forecast display for a selected time up to 20 minutes into the future.

In the en route center, the weather situation is depicted on the controllers' PVD and on a flow controller's console. The data for the PVD passes through the 9020 computer, whereas the flow controller console is driven directly from AWEP. Possible methods for indicating the storm cells and their parameters on the displays are described in Reference 5.

## 6.0 CONCLUSIONS AND RECOMMENDATIONS

Various candidate radar systems have been investigated to meet the needs for weather data by air traffic controllers. The objective is to provide data of sufficient quality to support detection and forecasting of hazardous weather associated with individual storm cells. The major conclusions reached during this investigation are:

a) The ASR operating at S-band can be adapted to meet the requirements derived in Reference 2 for thunderstorm detection by reflectivity processing.

b) If circular antenna polarization is employed for enhanced aircraft target visibility in precipitation, then an orthogonal polarization channel is necessary for weather detection. Thereby, the reduction in echo power and uncertainty in reflectivity of the primary polarization caused by rain drop ellipticity is avoided.

c) Although the MTD provides substantially better weather suppression than conventional radar processors, additional evidence should be gathered to determine the viability of operation exclusively with linear polarization.

d) Single RF channel operation for both aircraft and weather detection requires linear polarization and a compromise between $R^2$ and $R^4$ STC characteristics. A large portion of the aircraft signal processor can then be shared for weather detection.

e) At the price of a dual RF channel system, the conflicts on polarization and STC characteristics can be resolved.

f) Coherent processing in the weather channel facilitates separation of weather from ground clutter when the average radial velocity of the precipitation is favorable. Doppler filters such as in the MTD are appropriate for this function. If a conventional radar having two orthogonal polarization ports, e.g., the ASR(8), is to incorporate a weather channel, a noncoherent processor can be employed with lesser ground clutter discrimination based on the difference in Doppler spread relative to weather echoes.

g) The implementation of storm cell detection and forecasting requires additional hardware and software development effort as outlined below. Since the MTD may be deployed as part of the all-digital ARTS before these developments are complete, an interim procedure for extracting data for weather contour generation is suggested as a substitute for analog radar video. This type of presentation, however, falls short of meeting the needs of air traffic controllers for identification and forecasts of the small regions of hazardous turbulence.

h) To meet en route controllers' requirements for large area coverage and storm height data, a new weather radar is recommended. Economic considerations dictate a joint (FAA, NWS and AWS) national network of weather radars designed to meet the specifications of each user agency. The radar would operate at C-band with a 1° pencil beam and execute a sequence of elevation tilt scans. Coherent pulse-pair correlation would be incorporated to supply Doppler measurement data to NWS and AWS. A multiple staggered PRF structure is suggested to collect reflectivity observations at long range and accurate unambiguous Doppler data at shorter range.

The following tasks are recommended to pursue the work begun under this study for providing air traffic controllers with a useful severe weather situation display:

1. Develop a real-time demonstration system using an ASR to evaluate storm cell detection and forecasting to terminal controllers. To demonstrate weather processing only, the system need not be dual channel. A coherent processing capability with MTD-like filtering is desirable to minimize ground clutter effects.

2. Conduct weather radar and flight test experiments to confirm the turbulence/cell association, to refine forecast algorithms, and to explore the utility of Doppler information to improve hazard detection (See Reference 2.)

3. Continue the investigation of single vs dual channel operation by determining the appropriateness of linear polarization for the MTD under extreme precipitation and by establishing compromise STC characteristics.

4. Estimate implementation costs of single vs dual channel configuration and coherent vs noncoherent processing. These comparisons will aid in the selection of the most cost effective approach.

5. Conduct a cost/benefit study to determine the expected costs and benefits that may accrue from implementation of the design alternatives.

6. Implement an interim capability to extract weather data from the MTD for the all-digital ARTS.

7. Coordinate with NWS and AWS on specifications for a new weather radar leading to a field demonstration test system that serves en route controllers and also provides the necessary data inputs for the other agencies.

## APPENDIX A

### The Effect of Doppler Filters on Radar Weather Observations

Coherent MTI Doppler filtering permits the separation of ground clutter and weather echoes in the same range gate when the radial speed of the precipitation exceeds a certain limit. The radar echoes are in effect passed through a filter having a notch at the IF frequency to reject zero-velocity, i.e., ground clutter returns. Echoes from nearly tangentially moving weather are also suppressed in the zero-velocity notch. These effects are analyzed here with specific application to the MTD Doppler filter characteristics for ASR's.

Two points of view are taken both relating to the magnitude and direction of the wind velocity vector. The first considers wind-driven precipitation moving with a specific velocity through the radar coverage area. Whenever the radial velocity exceeds in magnitude a quantity $v_r$, determined by MTI filter characteristics and the spectral width of the weather, the weather echo is observable separate from ground clutter. The observable region corresponds to two angular sectors centered on the radar as indicated in the upper right diagram of Fig. A.1. The expression for the total observable angle is $2\pi - 4 \sin^{-1}(v_r/v_w)$ where $v_w$ is the wind speed. This equation is plotted as a percentage of a full circle in the figure.

The second point of view considers the precipitation velocity as an arbitrarily oriented vector referred to the radar line-of-sight (see lower-right diagram of Fig. A.1). The fraction of velocity orientations that lead to echoes observable through the MTI filter has exactly the form found above. Thus the graph in Fig. A.1 can be interpreted in either way, i.e., for a given $v_w$ the curve depicts the fraction of a full circle of 1) radar coverage or 2) velocity orientation for which the radial speed exceeds $v_r$.

A value of $v_r$ has been calculated for the MTD filter characteristics reported in Reference 3 under the assumption of weather spectral width (rms) of 2 m/s and 8 m/s. Non-zero Doppler filters were approximated by gaussian functions

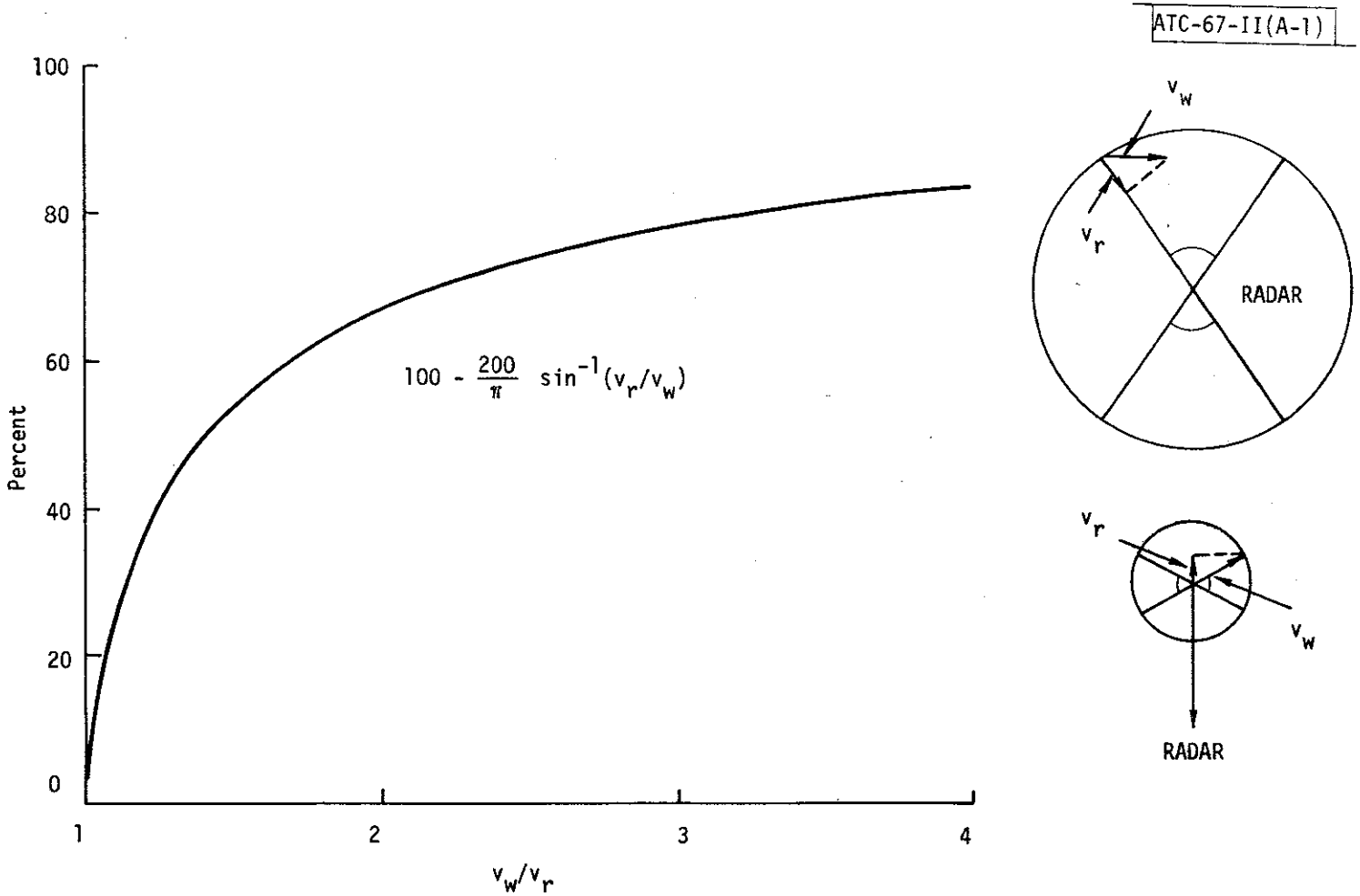


Fig. A-1 Fraction of 360° for which radial speed > $v_r$, wind speed = $v_w$.

and their power outputs in response to a gaussian power spectral density were summed. The weather spectrum was translated by an offset velocity $v_o$; the resulting attenuation is plotted in Fig. A.2. The criterion of observability is defined as an error of less than 3 dB in the measured precipitation reflectivity. The -3 dB point occurs near 7 m/s or 14 knots. This value is used for $v_r$ to denormalize the scales in Fig. A.1.

The successful separation of weather and ground clutter can be related to the wind speed for the computed example, e.g., 70% success is achieved when the average wind reaches 30 knots. However, the translational velocity of convective storms is often below 20 knots for which the success rate is near 50%.

We conclude that the ASR Doppler MTI filters cause serious degradation of weather data and that provisions must be made to include zero-velocity data in the reflectivity estimates when the radial weather motion is small. The recommended ASR weather processors incorporate this feature utilizing the Doppler spectral spread to distinguish obvious ground clutter from weather echoes.

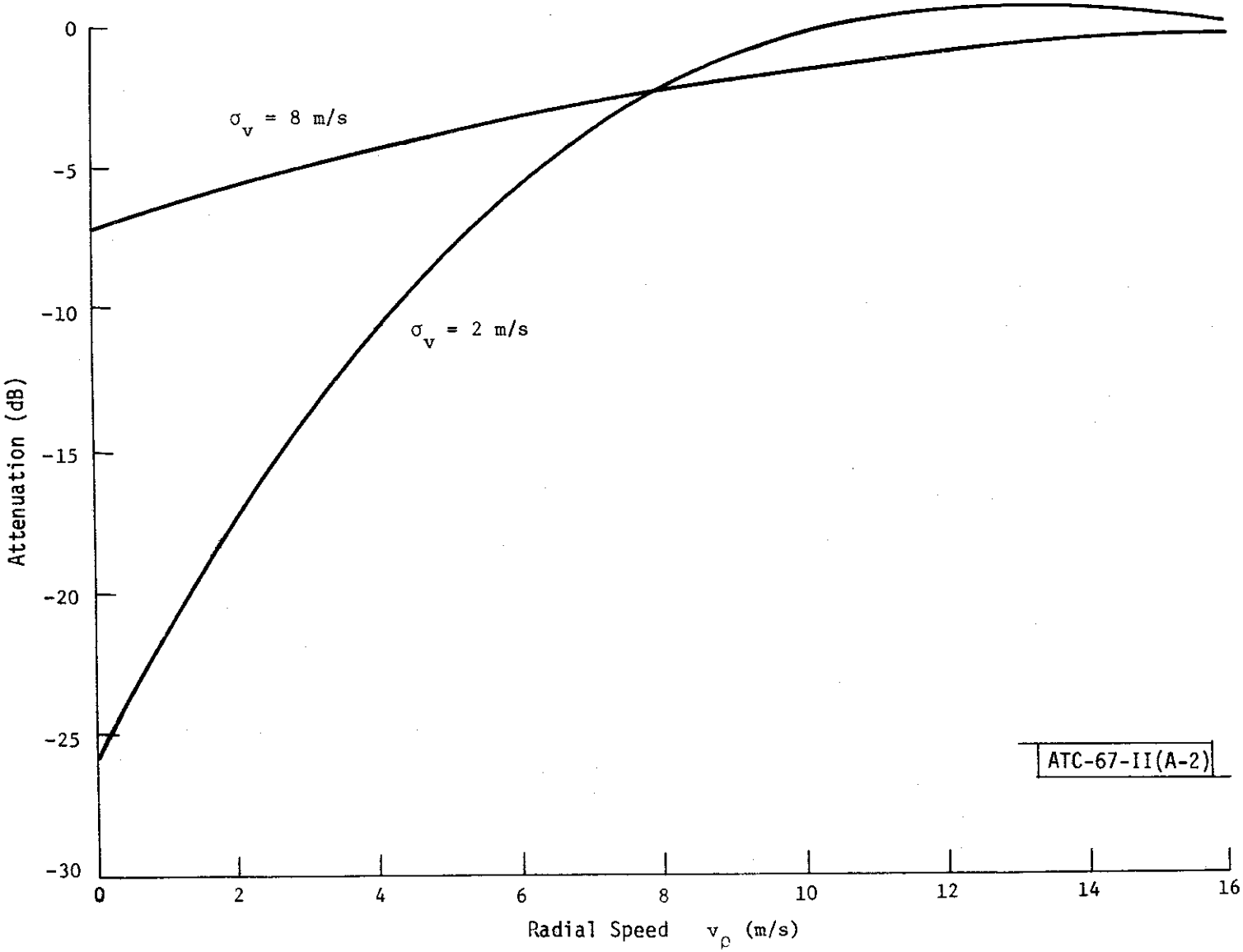


Fig. A-2 Attenuation of weather through MTD filters for rms spectral spread $\sigma_v$ = 2 and 8 m/s.

## APPENDIX B

### Averaging of Correlated Rayleigh Samples

The estimate of mean radar reflectivity is formed by averaging a sequence of samples of the radar echo. The fluctuation of the average establishes a limit on the precision of the measurement. The variance of the average, which is a useful measure of the fluctuations, is evaluated taking into account additive noise and correlation between samples. The radar echo is modelled as a complex gaussian process leading to a Rayleigh distributed envelope. Two cases are considered: the average of 1) square law, and 2) linear envelope samples.

Let x and y be the in-phase and quadrature components of the complex signal. These components are uncorrelated and their mean power is each equal to the mean power of the signal, i.e.,

$$\begin{aligned} s(t) &= x(t) \sin \omega t + y(t) \cos \omega t \\ \overline{s^2} &= (\overline{x^2} + \overline{y^2})/2 \\ \overline{s^2} &= \overline{x^2} = \overline{y^2} \end{aligned} \tag{1}$$

We define the envelope as

$$A = \sqrt{\frac{x^2 + y^2}{2}} \tag{2}$$

The reflectivity estimate is then derived from

$$\begin{aligned} \hat{A^2} &= \frac{1}{N} \sum_{i=1}^{M} A^2(t_i) \\ \hat{A} &= \frac{1}{N} \sum_{i=1}^{M} A(t_i) \end{aligned} \tag{3}$$

for the square law and linear case respectively.

Focussing first on the square-law case the mean value of the estimate is

$$\hat{A^2} = \overline{A^2} \tag{4}$$

and its mean square is

$$\overline{\left(\hat{A^2}\right)^2} = \frac{1}{N^2} \sum_{i=1}^{N} \sum_{j=1}^{N} \overline{A^2(t_i)A^2(t_j)} \tag{5}$$

Reference 6 gives the correlation function of the squared envelope in terms of the correlation of the complex components:

$$\overline{A_i^2(t_i)A^2(t_j)} = \left(\overline{A^2}\right)^2 [1 + \rho^2(t_i - t_j)]$$

$$\rho(\tau) = \overline{x(t)\, x(t+\tau)}/\overline{x^2} \tag{6}$$

Substituting in Eq. 5 with $\rho(t_i - t_j) = \rho_{i-j}$

$$\overline{\left(\hat{A^2}\right)^2} = \left(\overline{A^2}\right)^2 + \left(\frac{\overline{A^2}}{N}\right)^2 \sum_{i=1}^{N} \sum_{j=1}^{N} \rho_{i-j}^2$$

$$= \left(\overline{A^2}\right)^2 \left\{1 + \frac{1}{N^2} [N + 2(N-1)\rho_1 + 2(N-2)\rho_2 + \ldots]\right\} \tag{7}$$

The variance of the estimate is given by

$$\text{Var}\, \hat{A^2} = \overline{\left(\hat{A^2}\right)^2} - \left(\overline{A^2}\right)^2 \tag{8}$$

Making the assumption that $\rho_i$ diminishes rapidly enough and N is sufficiently large so that $(N-i)\rho_i \approx N\rho_i$ leaves

$$\text{Var } \hat{A}^2 = \frac{(\overline{A^2})^2}{N} [1 + 2\rho_1^2 + 2\rho_2^2 + \ldots 2\rho_{N-1}^2] = \frac{(\overline{A^2})^2}{N_{eq}}$$

where $N_{eq}$ is the equivalent or effective number of samples.
This form may be used to calculate the improvement in estimate error as a function of the number of samples N. Note that for uncorrelated samples $\rho_i = 0$, the variance decreases inversely with N as expected.

When additive receiver noise is present, the preceding is modified as follows: the correlation function of echo signal plus noise is

$$\rho(\tau) = [\overline{s^2}\rho_s(\tau) + \overline{n^2}\,\rho_n(\tau)]/(\overline{n^2} + \overline{s^2}) \tag{10}$$

and

$$\overline{A^2} = \overline{n^2} + \overline{s^2}$$

Since $t_i - t_j$ is the pulse repetition interval, we have $\rho_{n,i-j} = 0$ for $i \neq j$. Therefore (9) becomes

$$\begin{aligned} \text{Var } \hat{A}^2 &= \frac{1}{N}[(\overline{n^s} + \overline{s^2})^2 + 2(\overline{s^2})^2(\rho_{s,1}^2 + \rho_{s,2}^2 + \ldots)] \\ &= \frac{(\overline{s^2})^2}{N}[(1 + \text{SNR}^{-1})^2 + 2(\rho_{s,1}^2 + \rho_{s,2}^2 + \ldots)] \end{aligned} \tag{11}$$

A similar development must be carried out for the averaged linear envelope samples. The mean value and mean square values of the estimate are

$$\begin{aligned} \hat{A} &= \sqrt{\pi\overline{A^2}/2} \\ \overline{\hat{A}^2} &= \frac{1}{N^2}\sum_i \sum_j \overline{A(t_i)\,A(t_j)} \end{aligned} \tag{12}$$

From Reference 6 we get

$$\overline{A(t_i)A(t_j)} = \overline{A^2}\,[E(\rho_{i-j}) - \tfrac{1}{2}(1 - \rho_{i-j}^2)K(\rho_{i-j})] \qquad (13)$$

where K and E are the complete elliptic integrals of the first and second kind.

When substituting in Eq. (12), it is convenient to remove from the sum the constant corresponding to $E(0) = K(0) = \frac{\pi}{2}$.

Then

$$\overline{\hat{A}^2} = \frac{\overline{A^2}}{N^2} \sum_i \sum_j [E(\rho_{i-j}) - \tfrac{1}{2}(1 - \rho_{i-j}^2)K(\rho_{i-j}) - \tfrac{\pi}{4}] + \frac{\overline{A^2}\pi}{4} \qquad (14)$$

With $E(1)=1$, the variance becomes

$$\begin{aligned}\text{Var } A &= \overline{\hat{A}^2} - (\overline{\hat{A}})^2 \\ &= \frac{\overline{A^2}}{N}\left[1 - \tfrac{\pi}{4}\right] + \frac{\overline{A^2}}{N^2}\left\{2(N-1)\left[E(\rho_1) - \tfrac{1}{2}(1 - \rho_1{}^2)K(\rho_1) - \tfrac{\pi}{4}\right]\right. \\ &\quad \left. + 2(N-2)\left[E(\rho_2) - \tfrac{1}{2}(1 - \rho_2{}^2)K(\rho_2) - \tfrac{\pi}{4}\right] + \ldots\right\}\end{aligned}$$

Making the approximations used previously and including the noise through

$$\rho_i = \rho_{s,i}\,\frac{\overline{s^2}}{\overline{n^2} + \overline{s^2}} = \frac{\rho_{s,i}}{1 + \text{SNR}^{-1}}, \quad i \neq 0$$

yields

$$\text{Var } \hat{A} \approx \overline{s^2}\,\frac{(1 + \text{SNR}^{-1})}{4.66N}\left\{1 + 9.32 \sum_{i=1}^{N-1} [E(\rho_i) - (1-\rho_i{}^2)K(\rho_i) - \tfrac{\pi}{4}]\right\} \qquad (16)$$

To proceed with either Eq. (11) or (16), the correlation function is needed or its Fourier transform, the power spectral density of the weather echoes. The latter is generally taken to be gaussian with an rms width $\sigma_w$, i.e.,

$$W(\omega) = e^{-\omega^2/2\sigma_w^2} \qquad \sigma_w \text{ in rad/sec}$$

The corresponding correlation function is

$$\rho_s(\tau) = e^{-\tau^2\sigma_w^2/2}$$

For the specific example needed in the text we assume a conservatively low spectral spread of 0.7 m/s. At C-band ($\lambda$ = 0.053 m) this corresponds to $\sigma_w$ = 165 rad/sec. The pulse interval under consideration is $\tau_i$ = 3 msec, hence

$$\rho_1 = .885 \qquad \rho_2 = .61 \qquad \rho_3 = .33$$

For the square law average Eq. (11) gives

$$\text{Var } \hat{A^2} = \frac{(\overline{s^2})^2}{N}\left[(1 + \text{SNR}^{-1})^2 + 2.53\right]$$

For a nominal 10 dB SNR

$$\text{Var } \hat{A^2} = \frac{(\overline{s^2})^2}{N}(3.74)$$

The required number of samples for a given variance is 3.74 times the number for uncorrelated samples and no noise.

If the pulse spacing is increased to 6 ms,

$$\rho_1 = .61 \quad , \rho_2 = .14$$

$$\text{Var } \hat{A^2} = \frac{\overline{s^2}^2}{N'}\left[(1.1)^2 + 0.78\right] = \frac{\overline{s^2}}{N'}(1.98)$$

For a fixed-duration time average the number of pulses is reduced by one-half, N'=N/2, and therefore

$$\text{Var } \hat{A}^2 = \left(\frac{\overline{s^2}}{N}\right)^2 (3.96)$$

Due to the high correlation of successive samples, the increased spacing and corresponding reduction in number of pulses averaged has a small but noticeable effect on the variance.

Turning now to the linear envelope average, Eq. (16) gives for $\tau$ = 3 ms and SNR = 10 dB

$$\text{Var } \hat{A} = \frac{\overline{s^2}}{4.66N} (3.36)$$

At a spacing of 6 ms we get

$$\text{Var } \hat{A} = \frac{\overline{s^2}}{4.66N} (3.57)$$

The behavior of the square law and linear averages is similar; the differences are probably not significant in the light of model inaccuracies. For the design exercise in the main text $N = 3.5N_{eq}$ has been chosen.

## APPENDIX C
## Range Normalization

For a given precipitation reflectivity factor Z and complete antenna beam filling, the received power P(R) varies as $R^{-2}$ (see Ref. 1). This behavior is modified by the STC characteristic which can be expressed as a gain function g(R). If the storm cell top is limited to a height H, then the received power will decrease at long ranges due to partial beam filling. These factors can be incorporated in an equation for P(R):

$$P(R) = P(R_o) \frac{g(R)}{g(R_o)} \left(\frac{R_o}{R}\right)^2 \frac{\int_o^{\theta(R,H)} G(\theta)d\theta}{\int_o^{\theta(R_o,H)} G(\theta)d\theta} \qquad \text{(C-1)}$$

where

$G(\theta)$ = measured elevation beam pattern

$R_o$ = reference range where approximately complete beam filling occurs for a storm of height H

$\theta(R,H)$= elevation angle to top of storm at range R

From simple geometry it follows that

$$\theta(R,H) = \sin^{-1}\left(\frac{H}{R} - \frac{R}{2a_e}\right)$$

The second term in parenthesis correct for earth curvature with an effective earth radius $a_e$.

If one assumes a nominal cell height H for which the range normalization is to be optimized, all the elements of Eq. (C-1) can be evaluated. It is then possible to obtain a tabulation of P(R) vs R whose inverse becomes the desired range normalization. This normalization will compensate for range loss, STC and antenna elevation pattern to yield a measurement proportional to reflectivity factor.

## ACKNOWLEDGEMENTS

Significant contributions to the work reported were made by R. K. Crane. Suggestions and helpful criticisms from I.G. Stiglitz, C.E. Muehe, S.I. Krich, M. Labitt and R.M. O'Donnell are also acknowledged.

## REFERENCES


1. L.J. Battan, Radar Observation of the Atmosphere, Univ. of Chicago (1973).

2. R.K. Crane, "Radar Detection of Thunderstorm Hazards for Air Traffic Control Volume I: Storm Cell Detection," Project Report ATC-67, Vol.I, Lincoln Laboratory, M.I.T. (7 October 1976).

3. W.H. Drury, "Improved MTI Radar Signal Processor," Project Report ATC-39, Lincoln Laboratory, M.I.T. (3 April 1975).

4. H.L. Groginsky, "Pulse Pair Estimation of Doppler Spectrum Parameters," 15th Radar Meteor. Conf. (Oct. 1972) pp. 233-236.

5. S.I. Krich and S.M. Sussman, "A Concept and Plan for the Development of a Weather Support Subsystem for Air Traffic Control," Project Report ATC-64, Lincoln Laboratory, M.I.T. (16 April 1976).

6. J.L. Lawson and G.E. Uhlenbeck, Threshold Signals, McGraw Hill (1950).

7. J.S. Marshall and W. Hitschfeld, "Interpretation of the Fluctuating Echo from Randomly Distributed Scatterers," Part I. Can. J. Phys. v. 31 (1953) pp. 962-994.

8. K.S. Miller and M.M. Rockwarger, "A Covariance Approach to Spectral Moment Estimation," IEEE Trans. on Info, Th. v. IT-18, n. 5, (Sept. 1972) pp.588-596.

9. F.E. Nathanson, Radar Design Principles, McGraw-Hill (1969) p. 345.

10. R.M. O'Donnell, private communication.

11. D. Sirmans and B. Bumgarner, "Numerical Comparison of Five Mean Frequency Estimators," J. Appl. Meteor. v. 14 (Sept. 1975) pp. 991-1003,

12. M.P. Warden and E.J. Dodsworth, "A Review of Clutter, 1974," Royal Radar Establishment, Malvern, Tech. Note 783 (Sept. 1974).

13. "Static Radar Cross Section of Light Aircraft," FAA-RD-73-192 (Vols. I, II, III) (Dec. 1973).

14. First Draft of ASR-( ) DABS Backup Radar Development Plan, FAA Radar Radar Study Group under ARD-240.